AUTOIMMUNITY

Epstein-Barr virus reprograms autoreactive B cells as antigen-presenting cells in systemic lupus erythematosus

Shady Younis[1,2]*, Salvinaz I. Moutusy[1,2], Sajede Rasouli[1,2], Shaghayegh Jahanbani[1,2], Mahesh Pandit[1,2], Xiaohao Wu[1,2], Suman Acharya[1,2], Orr Sharpe[1,2], Tilini U. Wijeratne[1,2], Marlayna L. Harris[1], Emily Y. Yang[1], Yashaar Chaichian[1], Shima Parsafar[1], Matthew C. Baker[1], John B. Harley[3,4], Eric Meffre[1], Lawrence Steinman[5,6], Ann Marshak-Rothstein[7], Judith A. James[8,9], Olivia M. Martinez[10], Paul J. Utz[1,11], Dana E. Orange[12,13], Tobias V. Lanz[1,11], William H. Robinson[1,2,11]*

Systemic lupus erythematosus (SLE) is a systemic autoimmune disease characterized by antinuclear antibodies (ANAs). Epstein-Barr virus (EBV) infection has been epidemiologically associated with SLE, yet its role in pathogenesis remains incompletely defined. Here, we developed an EBV-specific single-cell RNA-sequencing platform and used it to demonstrate that EBV infection reprograms autoreactive antinuclear antigen B cells to drive autoimmunity in SLE. We demonstrated that, in SLE, EBV$^+$ B cells are predominantly CD27$^+$CD21^{low} memory B cells that are present at increased frequencies and express *ZEB2*, *TBX21* (T-bet), and antigen-presenting cell transcriptional pathways. Integrative analysis of chromatin immunoprecipitation sequencing (ChIP-seq), assay for transposase-accessible chromatin sequencing (ATAC-seq), and RNA polymerase II occupancy data revealed EBV nuclear antigen 2 (EBNA2) binding at the transcriptional start sites and regulatory regions of *CD27*, *ZEB2*, and *TBX21*, as well as the antigen-presenting cell genes demonstrated to be up-regulated in SLE EBV$^+$ B cells. We expressed recombinant antibodies from SLE EBV$^+$ B cells and demonstrated that they bind prototypical SLE nuclear autoantigens, whereas those from healthy individuals do not. We further found that SLE EBV$^+$ B cells can serve as antigen-presenting cells to drive activation of T peripheral helper cells with concomitant activation of related EBV$^-$ antinuclear double-negative 2 B cells and plasmablasts. Our results provide a mechanistic basis for EBV being a driver of SLE through infecting and reprogramming nuclear antigen-reactive B cells to become activated antigen-presenting cells with the potential to promote systemic disease–driving autoimmune responses.

INTRODUCTION

Epstein-Barr virus (EBV) is among the most common human viruses and is transmitted primarily through saliva (*1*). Infection typically occurs during childhood, adolescence, or young adulthood, and EBV is the leading cause of infectious mononucleosis ("mono"). By adulthood, more than 94% of humans have been infected (*1*). EBV infection has been linked to systemic lupus erythematosus (SLE) through serologic, cellular, and molecular data (*2*, *3*). Moreover, EBV infection has been epidemiologically linked to SLE on the basis of the high prevalence of anti-EBV nuclear antigen 1 (EBNA1) antibodies in pediatric and adult patients with SLE (*4*, *5*) and observations that EBV lytic reactivation is associated with transition from preclinical to clinical SLE (*6*) and with SLE disease activity (*7*). Nevertheless, how EBV might cause or promote SLE remains incompletely defined.

EBV is a double-stranded DNA (dsDNA) virus belonging to the herpesvirus family (Herpesviridae), specifically the gammaherpesvirus subfamily (*1*, *8*). EBV infects epithelial cells and B cells and establishes lifelong infection with limited viral gene expression. EBV-infected B cells are predominantly memory B cells, and distinct latency programs (latency I, II, and III) are mediated by expression of distinct sets of EBV genes that promote immune evasion and viral persistence (*1*, *8*).

Investigation of the mechanisms by which EBV might promote SLE has been hampered by biological and technological challenges, including the complex EBV life cycle that includes multiple latency phases and lytic reactivation (*1*, *8*); the low expression of the limited set of EBV latency genes (*1*); and the low frequency of EBV$^+$ B cells in blood, with a previously estimated mean of 3.5 EBV$^+$ B cells per million B cells in SLE (*9*, *10*). Furthermore, patients with SLE exhibit prominent abnormalities in their B cell compartment, including antinuclear antigen EBV$^-$ double-negative 2 B cells [DN2, a subset of age-associated B cells (ABCs); (*11*–*15*)] and plasmablasts, which can represent greater than 1% of blood B cells (*16*, *17*). The exact phenotype, function, and B cell receptor (BCR) specificity of rare EBV$^+$ B cell clones are unknown, as is their potential to shape the broad autoreactive antinuclear antigen B cell response observed in SLE.

A variety of mechanisms have been proposed by which EBV could promote autoimmunity and SLE, including EBV-mediated molecular

[1]Division of Immunology and Rheumatology, Stanford University, Stanford, CA 94305, USA. [2]VA Palo Alto Health Care System, Palo Alto, CA 94304, USA. [3]Research Service, US Department of Veterans Affairs Medical Center, Cincinnati, OH 45220, USA. [4]Cincinnati Education and Research for Veterans Foundation, Cincinnati, OH 45220, USA. [5]Department of Neurology and Neurological Sciences, Stanford University, Stanford, CA 94305, USA. [6]Department of Pediatrics, Stanford University, Stanford, CA 94305, USA. [7]Department of Medicine, University of Massachusetts School of Medicine, Worcester, MA 01655, USA. [8]Arthritis and Clinical Immunology Program, Oklahoma Medical Research Foundation, Oklahoma City, OK 73104, USA. [9]Department of Medicine, University of Oklahoma Health Sciences Center, Oklahoma City, OK 73104, USA. [10]Department of Surgery, Stanford University, Stanford, CA 94305, USA. [11]Institute for Immunity, Transplantation, and Infection, Stanford University, Stanford, CA 94305, USA. [12]Rockefeller University, New York, NY 10065, USA. [13]Hospital for Special Surgery, New York, NY 10021, USA.
*Corresponding author. Email: wrobins@stanford.edu (W.H.R.); syounis@stanford.edu (S.Y.)

mimicry (*18*, *19*); functional mimicry through Epstein-Barr virus interleukin 10 (vIL10), latent membrane protein 1 (LMP1), or latent membrane protein 2a (LMP2a) (*3*, *20*); autoimmune promoting strains of EBV (*21*); EBV nuclear antigen 2 (EBNA2)–mediated dysregulation of autoimmune susceptibility genes (*22*); EBV-promoted B cell escape from tolerance (*23*–*25*); EBV-driven development of memory B cells (*23*); dysregulated intrinsic B cell control of EBV gene expression resulting in lytic reactivation (*26*, *27*); immune evasion by EBV-infected B cells (*1*, *8*); and insufficient T and natural killer cell control of EBV-induced autoimmune responses (*28*). Recently, it was shown that EBV contributes to the pathogenesis of multiple sclerosis by expanding oligoclonal T-bet$^+$CXCR3$^+$ B cells that home to the central nervous system and can attract T cells (*29*). Here, we developed tools for EBV-specific single-cell RNA sequencing (scRNA-seq) and applied these methods to sequence the B cell repertoires of patients with SLE and healthy controls (HCs).

RESULTS

EBV-seq enables detection of EBV$^+$ B cells

A major challenge in the field has been the inability to directly characterize EBV$^+$ B cells to define their role in autoimmunity. In autoimmunity, EBV$^+$ B cells are rare, EBV gene expression is frequently below the threshold for detection by scRNA-seq, and nonpolyadenylated EBV RNAs including Epstein-Barr virus–encoded small RNAs (EBERs) are not captured using the 10× Genomics scRNA-seq platform. To overcome these challenges and to enable multimodal scRNA-seq of EBV$^+$ B cells, we combined 23 primers specific for 21 EBV genes into our 10× Genomics droplet-based scRNA-seq workflow (EBV-seq; Fig. 1, A and B, and table S1). The EBV primers are incorporated through reverse transcription and used for amplification polymerase chain reactions (PCRs) and contain a sequencing-compatible PCR "handle" to enable amplification of the EBV-specific libraries alongside human BCR and whole transcriptome libraries. When tested on the EBV$^+$ B cell line Raji, EBV-seq provided an approximately fourfold increase in the unique molecular identifier (UMI) gene counts that uniquely mapped to the EBV genome compared with standard scRNA-seq methodology (fig. S1, A and B). We next tested EBV-seq on an SLE blood B cell sample, and EBV-seq detected EBV$^+$ B cells on the basis of EBV gene UMI counts, whereas standard scRNA-seq failed to detect sufficient EBV gene UMI counts to identify EBV$^+$ B cells (Fig. 1C and fig. S1C).

EBV$^+$ B cells are increased in frequency in the blood of patients with SLE and are predominantly CD27$^+$CD21^{low} memory B cells

Using combined EBV-seq, CITE-seq (cellular indexing of transcriptomes and epitopes by sequencing), BCR-seq, and scRNA-seq, we sequenced the EBV genes, BCR repertoires, and transcriptomes of

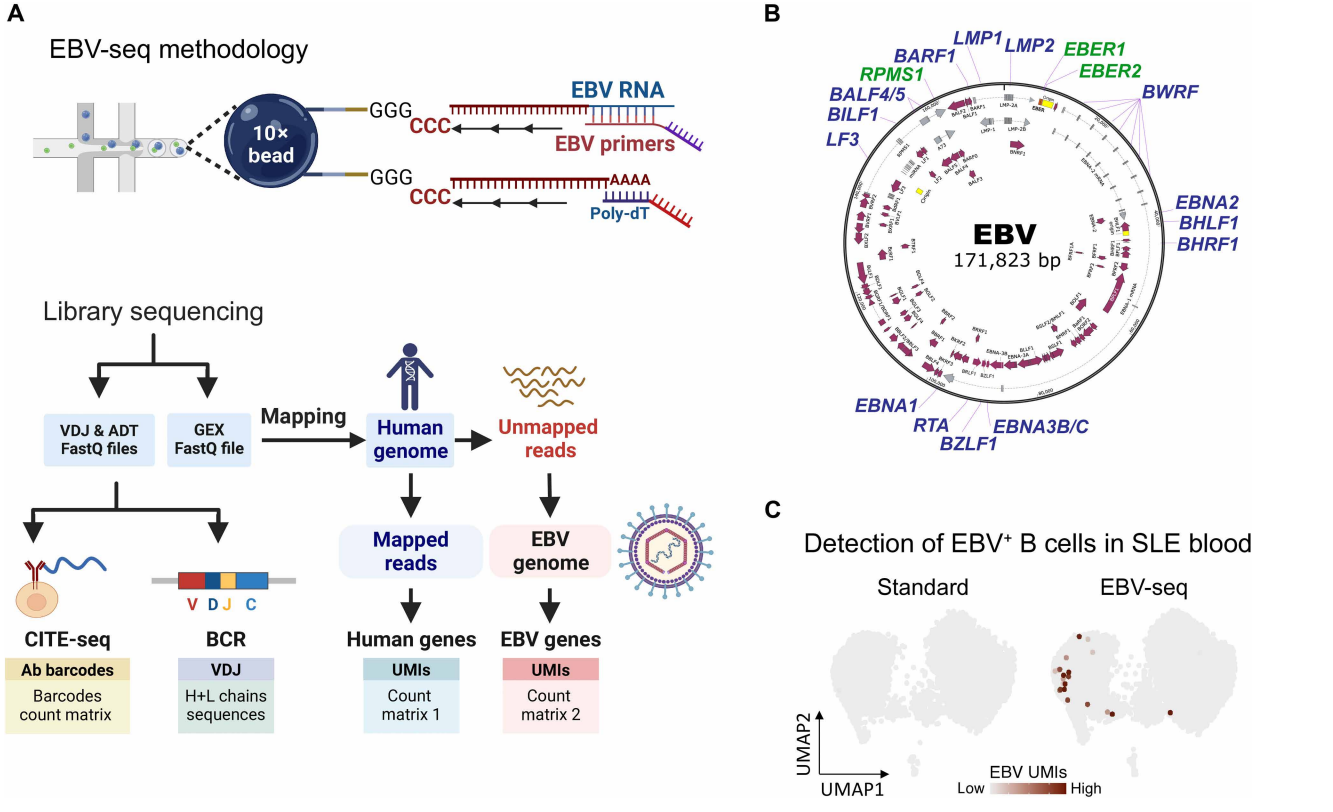

Fig. 1. EBV-seq enables identification of EBV-infected B cells. (**A**) An EBV-seq primer design was incorporated into a 10x Genomics bead-based scRNA-seq workflow that included CITE-seq performed using oligonucleotide-barcoded Abs specific for the prototypical markers for B cell subsets. BCR sequencing was performed by analysis of the expressed variable diversity and joining (VDJ) immunoglobulin genes, followed by analysis of immunoglobulin heavy (H) and light (L) chain gene expression. (**B**) Shown is the EBV genome annotated with the EBV genes (blue font) and small noncoding RNAs (green font) for which primers were included in EBV-seq. (**C**) Comparison of standard 10x Genomics scRNA-seq with EBV-seq 10x Genomics scRNA-seq for detection of EBV$^+$ B cells in a PBMC sample from a patient with SLE; EBV UMI counts are represented by intensity of brown dots. ADT, antibody-derived tag.

blood B cells from patients with SLE ($n = 11$) and matched HCs ($n = 10$) (Fig. 2A and table S2). EBV$^+$ B cells were identified on the basis of expression of EBV gene UMI counts, and the number of EBV$^+$ B cells was normalized to the total number of sequenced B cells in each sample. In patients with SLE, we identified a mean EBV$^+$ B cell frequency of ~25 per 10,000 sequenced B cells, ranging from 2.3 to 82 EBV$^+$ B cells per 10,000 sequenced B cells in SLE. In contrast, we only detected a mean EBV$^+$ B cell frequency of 1 per 10,000 sequenced B cells in HCs, ranging from 0 to 3 EBV$^+$ B cells per 10,000 sequenced B cells in HCs. Patients with SLE harbored ~25-fold higher proportions of EBV$^+$ blood B cells compared with HCs ($P < 0.001$, by Wilcoxon rank sum test; Fig. 2B). Parallel analysis by EBER–flow cytometry demonstrated a correlation between EBV$^+$ cell frequencies measured by EBV-seq and EBER–flow cytometry (fig. S1, D and E).

We next integrated the EBV mapped reads with human gene expression and clustered the cells on the basis of differentially expressed genes (DEGs) and proteins (CITE-seq) using an unsupervised approach. The clusters were annotated on the basis of the expression of genes and proteins encoding prototypical markers of each B cell subset (*16*): naïve B cells [CD27$^-$IgD$^+$ (immunoglobulin D–positive); DN1 B cells [CD27$^-$IgD$^-$CD11c$^-$T-bet$^-$FCRL5$^-$ (FcRL5, Fc receptor like 5)]; DN2 B cells [CD27$^-$IgD$^-$CD11c$^+$Zeb2$^+$T-bet$^+$FCRL5$^+$ (Zeb2, zinc finger E-box binding homeobox 2)], which represent a subset of age-associated B cells (ABCs) (*13*–*15*, *30*); memory B cells (CD27$^+$IgD$^-$); CD27$^+$CD21^{low} memory B cells (which are CD27$^+$T-bet^{low}Zeb2^{low} FCRL5^{low} and thus are distinct from CD27$^+$CD21$^-$Zeb2$^+$T-bet$^+$ FCRL5$^+$ atypical B cells) (*11*–*15*); and plasmablasts (CD20$^-$CD38^{++} CD27$^+$) (Fig. 2C, fig. S2, and table S3). Analysis of EBV gene UMI counts revealed that the EBV$^+$ B cells in blood samples from patients with SLE were predominantly within the CD27$^+$CD21^{low} memory B cell subset and were also modestly elevated in the unswitched memory B cell and Ki67$^-$ plasmablast populations (Fig. 2, D to F), consistent with prior studies reporting latent EBV in memory B cells both in patients with SLE and healthy individuals (*8*–*10*). Small numbers of EBV$^+$ B cells were observed in the follicular B, switched memory B, and DN1 (*14*, *15*) B cell subsets in SLE (Fig. 2F).

SLE EBV$^+$ B cells are predominantly in latency phase, with a small number of cells expressing lytic reactivation genes

To define the latency state of EBV$^+$ B cells in SLE, we mapped EBV gene expression onto established expression patterns that define EBV latency versus lytic reactivation (*1*, *8*). The SLE EBV$^+$ CD27$^+$CD21^{low} memory B cells and other EBV$^+$ B cells were predominantly in latency 0 to 1 phases on the basis of expression of EBERs (*29*) or EBNA1 in the absence of EBV genes characteristic of latency 2 to 3 or lytic reactivation ($P < 0.01$, by Wilcoxon rank sum test; Fig. 2G and fig. S3). In SLE but not in HC B cells, we detected a small number of B cells expressing EBV lytic reactivation gene products in CD27$^+$CD21^{low} memory, DN2, unswitched memory B, plasmablast, and naïve B cells (Fig. 2G and fig. S3).

Activation and antigen-presenting cell pathways are up-regulated in EBV$^+$ CD27$^+$CD21^{low} memory B cells in blood samples from individuals with SLE

To gain insights into the impact of EBV on host B cell gene expression, given that EBV$^+$ B cells were predominantly CD27$^+$CD21^{low}, we measured the DEGs in SLE EBV$^+$ versus SLE EBV$^-$ B cells within the CD27$^+$CD21^{low} memory B cell subset (Fig. 3, A and B, and fig. S4). Pathway analysis demonstrated that SLE EBV$^+$ CD27$^+$CD21^{low} memory B cells exhibited up-regulation of transcriptional programs associated with viral processes, antigen-presenting cell (APC) function, B cell activation, and interferon-stimulated genes as compared with EBV$^-$ CD27$^+$CD21^{low} B cells (Fig. 3C and table S4). We also compared the transcriptomes of EBV$^+$ CD27$^+$CD21^{low} memory B cells in SLE samples versus HC samples and demonstrated that the EBV$^+$ CD27$^+$CD21^{low} memory B cells in SLE also exhibited up-regulation of T cell activation, APC function, B cell activation, and interferon pathways as compared with HC (Fig. 3, D to F, and fig. S4).

Among the most up-regulated genes in SLE EBV$^+$ CD27$^+$CD21^{low} memory B cells was *CD70* (Fig. 3, B and E), a marker of mature B cells recently primed by antigen and capable of producing high-affinity antibodies upon T cell–dependent stimulation (*31*). In addition, genes involved in antigen processing and presentation, including *IFI30*, *TAP2*, and *PSMB6*, were up-regulated in SLE EBV$^+$ CD27$^+$CD21^{low} memory B cells (Fig. 3B, fig. S4, and table S4). Interferon gamma-inducible protein 30 (IFI30) facilitates the reduction of disulfide bonds in internalized antigens, enhancing their processing for major histocompatibility complex (MHC) class II presentation (*32*); TAP2 [transporter 2, ATP (adenosine 5′-triphosphate) binding cassette subfamily B member] is essential for transporting peptides into the endoplasmic reticulum for MHC class I loading (*33*); and PSMB6 (proteasome subunit beta type 6) is a key component of the proteasome involved in generating antigenic peptides (*34*). The coordinated up-regulation of these genes suggests that EBV$^+$ B cells have an enhanced capacity to process and present autoantigens. Key signaling molecules essential for BCR signaling, including *BTK*, *BLNK*, *JAK3*, and *PIK3R1*, were also overexpressed, indicating heightened activation of downstream pathways critical for B cell function.

Furthermore, the ectonucleotidase-encoding genes *NT5E* (encoding CD73) and *ENTPD1* (encoding CD39), along with *TGFB1*, were up-regulated in EBV$^+$ B cells (fig. S4 and table S4). Both CD73 and CD39 catalyze the conversion of extracellular ATP into immunosuppressive adenosine, thereby modulating immune responses (*35*). Recent studies reported that elevated transforming growth factor–β (TGF-β) can impair anti-EBV T cell responses, ultimately facilitating EBV reactivation. The concurrent up-regulation of *TGFB1* and *NT5E* in SLE EBV$^+$ B cells supports a model in which these molecules establish an immunosuppressive microenvironment that restricts T cell surveillance, thereby promoting the immune escape and persistence of EBV$^+$ B cells.

Activation and APC pathways are up-regulated in EBV$^+$ SLE B cells across B cell subsets

To further characterize the dysregulated EBV$^+$ B cells in SLE, we characterized DEGs across B cell subsets and the pathways represented by these genes. We identified up-regulated antigen processing and presentation, regulation of T cell activation, B cell activation, EBV infection, and response to virus transcriptional pathways in SLE EBV$^+$ B cells across B cell subsets (Fig. 4A). On the basis of identification of up-regulated antigen processing and presentation, B cell activation, and response to virus pathways in SLE EBV$^+$ B cells, we next generated transcriptional modules representing APC function, B cell activation, interferon responses, and cellular proliferation. As compared with SLE EBV$^-$ or HC EBV$^+$ B cells, bulk SLE EBV$^+$ B cells exhibited increased APC function, B cell activation, and interferon response pathways (Fig. 4B). Analysis of EBV$^+$ B cells across B cell subsets demonstrated that SLE EBV$^+$ unswitched memory B cells, switched memory B cells, CD27$^+$CD21^{low} B cells, DN1 B cells,

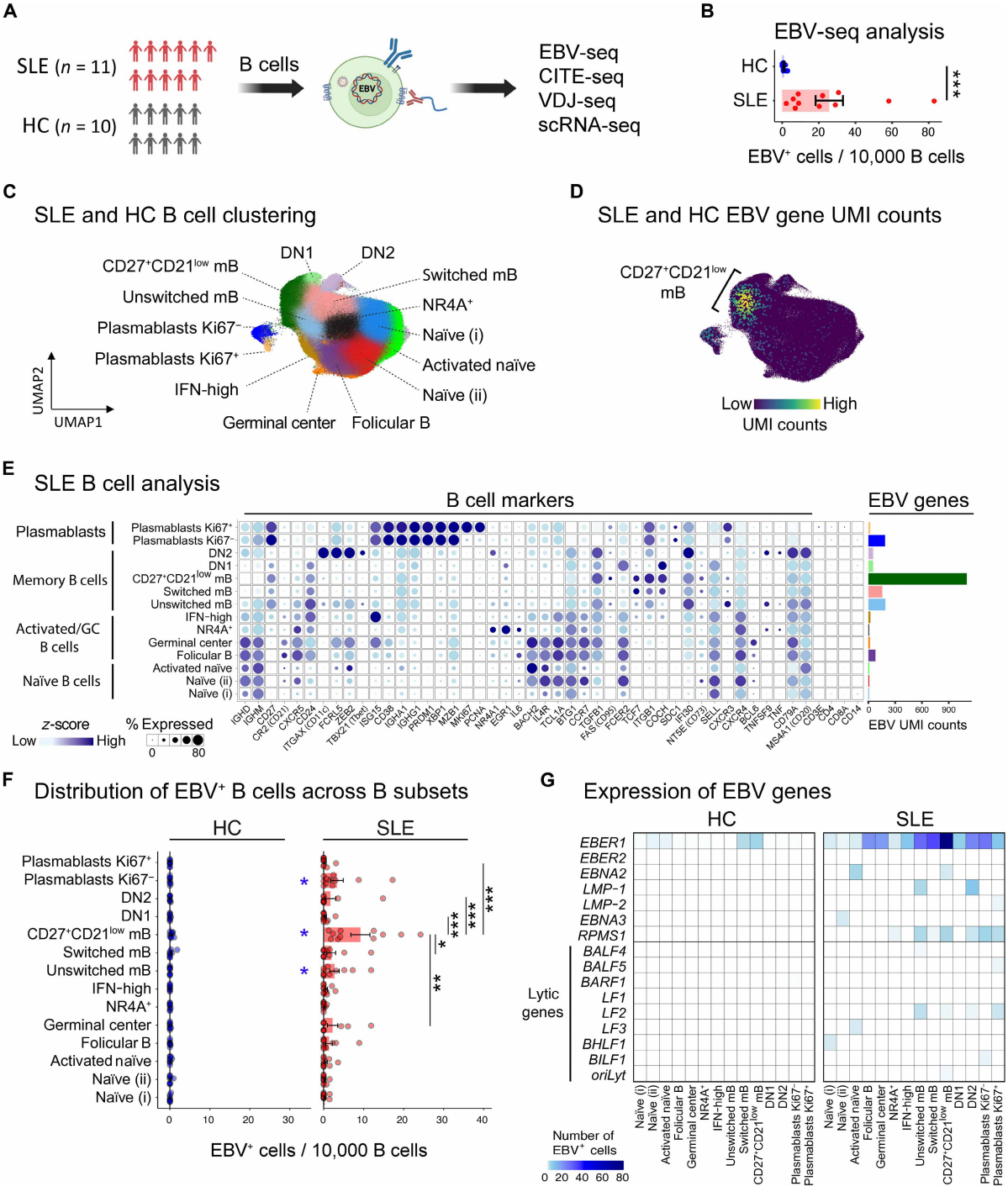

Fig. 2. EBV-seq analysis of blood from patients with SLE identified EBV$^+$ B cells predominantly in latency with some B cells expressing lytic reactivation genes. (**A**) Combined EBV-seq, CITE-seq, VDJ-seq, and scRNA-seq were used to sequence B cells isolated from SLE ($n = 11$) and HC ($n = 10$) PBMC samples. (**B**) Number of EBV$^+$ B cells detected in SLE and HC blood, normalized to 10,000 B cells. Each dot represents one individual, and bars represent means ± SEM. ***$P < 0.001$, by Wilcoxon rank sum test. (**C**) Unsupervised clustering based on DEGs in the sequenced SLE and HC B cells, with annotation of B cell subsets. (**D**) EBV gene UMI counts in the sequenced SLE and HC B cells. (**E**) SLE blood B cell marker expression. The bar graph represents the total EBV UMI counts detected in each B cell subset. (**F**) Distribution of EBV$^+$ B cells across B cell subsets in HC and SLE PBMCs. Data are presented as the normalized number of EBV$^+$ B cells per 10,000 B cells of the corresponding B cell subset. Bars represent means ± SEM. Statistical significance was determined by Kruskal-Wallis test with *P* values adjusted for multiple testing using the Benjamini-Hochberg method (*$P < 0.05$; **$P < 0.01$; ***$P < 0.001$). Blue asterisks indicate differences in EBV$^+$ B cell frequencies between HCs and patients with SLE within each subset, and black asterisks indicate pairwise comparisons of CD27$^+$CD21^{low} B cells against other EBV$^+$ subsets in SLE. (**G**) Frequencies of EBV gene UMI counts in B cell subsets from HCs and patients with SLE; EBV genes from which UMI gene counts were not detected are not displayed. The heatmap represents the number of EBV$^+$ B cells per 10,000 B cells per B cell subset. IFN, interferon; mB, memory B cells; GC, germinal center; NR4A, nuclear receptor subfamily 4A.

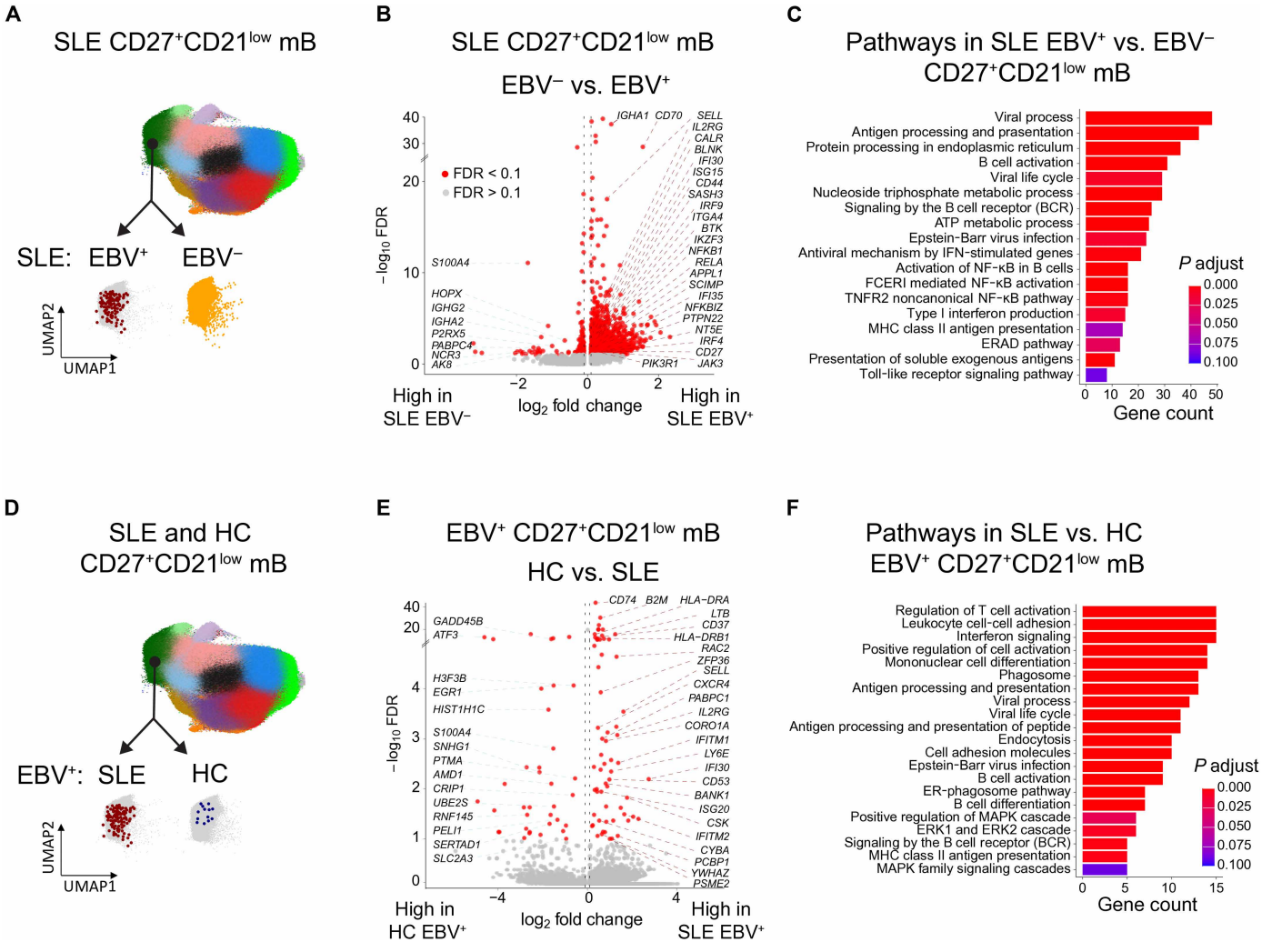

Fig. 3. SLE EBV$^+$ CD27$^+$CD21^{low} memory B cells exhibit activation as APCs. (**A**) Differential gene expression analysis of SLE blood EBV$^+$ versus EBV$^-$ CD27$^+$CD21^{low} memory B cells. (**B**) Volcano plot of DEGs in SLE EBV$^+$ versus EBV$^-$ CD27$^+$CD21^{low} memory B cells. (**C**) Activated pathways of the DEGs in SLE EBV$^+$ versus EBV$^-$ CD27$^+$CD21^{low} memory B cells. (**D**) Differential gene expression analysis of EBV$^+$ CD27$^+$CD21^{low} memory B cells in SLE versus HC blood. (**E**) Volcano plot of DEGs in EBV$^+$ CD27$^+$CD21^{low} memory B cells in SLE versus HC blood. (**F**) Activated pathways of the DEGs in EBV$^+$ CD27$^+$CD21^{low} memory B cells in SLE versus HC blood. ER, endoplasmic reticulum; ERAD, endoplasmic reticulum–associated protein degradation; FCERI, Fc epsilon receptor Ia; MAPK, mitogen activated kinase-like protein; TNFR2, tumor necrosis factor receptor 2.

DN2 B cells, and Ki67$^-$ plasmablasts all exhibited increased APC activity, B cell activation, or interferon module expression as compared with SLE EBV$^-$ or HC EBV$^+$ B cells ($P < 0.05$, by Mann-Whitney U test with multiple testing correction using the Benjamini-Hochberg method), whereas the proliferation transcriptional module was low across the groups (except for Ki67$^+$ plasmablasts) (Fig. 4, C to E, and fig. S5). Our data collectively demonstrate that, across B cell subsets, SLE EBV$^+$ B cells are activated as APCs.

EBV$^+$ CD27$^+$CD21^{low} memory B cells exhibit differentiation toward plasmablasts

To elucidate the lineage relationships among EBV$^+$ B cells across B cell subsets, we performed unbiased trajectory analysis based on RNA velocity analysis (*36*, *37*). The resulting SLE EBV$^+$ B cell trajectory map predicted the future states of individual SLE EBV$^+$ B cells on the basis of their spliced and unspliced mRNA content (Fig. 4F). In SLE, the EBV$^+$ naïve (ii) and naïve (i) B cells exhibit directional flow toward the CD27$^+$CD21$^-$ memory B cluster, consistent with the possibility that, in SLE, EBV infects and reprograms CD21$^+$ naïve B cells to differentiate into EBV$^+$ CD27$^+$CD21$^-$ memory B cells (Fig. 4F). Moreover, the EBV$^+$ CD27$^+$CD21^{low} memory B cluster exhibited a pronounced directional flow toward the proliferating plasmablast subset, indicating that EBV$^+$ CD27$^+$CD21^{low} memory B cells are primed to differentiate into Ki67$^+$ plasmablasts. These observations identify key transitional states and suggest that EBV$^+$ CD27$^+$CD21^{low} memory B cells might differentiate into EBV$^+$ plasmablasts in SLE.

EBNA2 binds regions implicated in transcriptional and epigenetic regulation of *CD27*, *ZEB2*, and *TBX21* (T-bet), as well as genes involved in antigen presentation

To gain further insights into the transcriptional dysregulation in EBV$^+$ B cells in SLE, we characterized expression of B cell subset markers and transcription factors (TFs) in EBV$^+$ and EBV$^-$ B cells

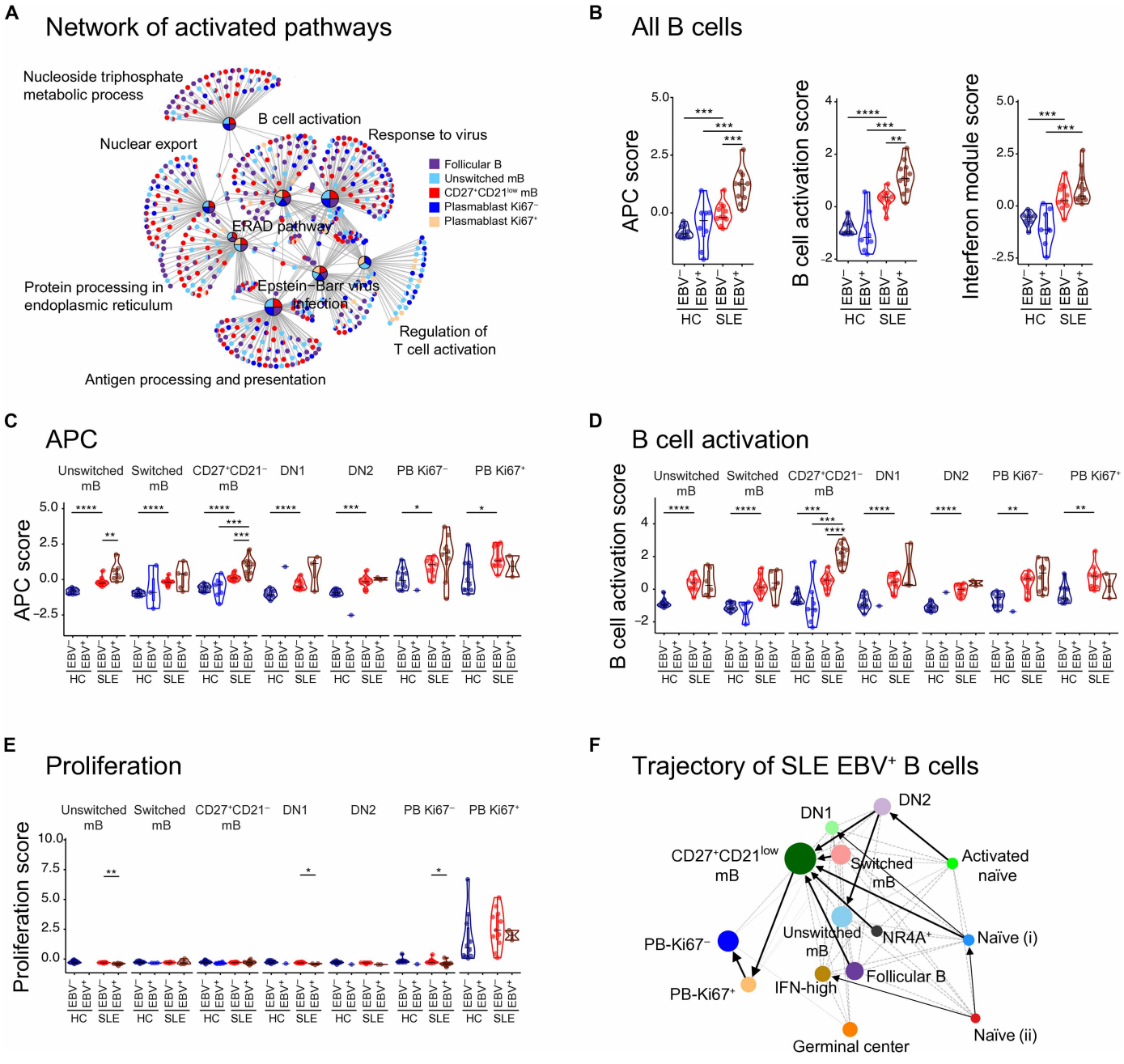

Fig. 4. EBV$^+$ B cells in SLE harbor distinct transcriptional programs and developmental trajectories toward CD27$^+$CD21^{low} memory and plasmablast phenotypes. (**A**) Network analysis of DEGs in EBV$^+$ cells as compared to EBV$^-$ B cell subsets. (**B**) B cell activation score, APC score, and interferon score across all B cells. Scores were defined as described in Materials and Methods. (**C** to **E**) APC score (C), B cell activation score (D), and interferon score (E) of the unswitched memory B cell, switched memory B cell, CD27$^+$CD21^{low} memory B cell, DN2 B cell, DN1 B cell, nonproliferating Ki67$^-$ plasmablast (PB), and proliferating Ki67$^+$ plasmablast subsets in EBV$^+$ and EBV$^-$ B cells in peripheral blood from individuals with SLE and HCs. *$P < 0.05$; **$P < 0.01$; ***$P < 0.001$; ****$P < 0.0001$, by Mann-Whitney *U* test with Benjamini-Hochberg correction for multiple testing. (**F**) Trajectory analysis of EBV$^+$ B cells. Solid arrows indicate inferred directional flows or transitions among subsets as computed by RNA velocity.

and observed up-regulation of *CD27*, *ZEB2*, *TBX21*, and APC genes in EBV$^+$ B cells across B cell subsets (Fig. 5A). Given that EBNA2 is implicated in regulating SLE susceptibility genes (*22*) and is specifically expressed in latency 3 (*1*), we classified SLE EBV$^+$ B cells on the basis of expression of latency phase–associated RNAs and genes. Because of limitations in the sensitivity of EBV-seq for detecting EBV RNAs and genes, we used groups of latency phase–associated EBV RNAs and genes to classify EBV$^+$ B cells. We classified EBV$^+$ B cells expressing only EBERs as being in latency 0 to 1; EBNA2, LMP1, LMP2, or EBNA3 as being in latency 2 to 3; and lytic genes as being in lytic phase (Fig. 5B). SLE EBV$^+$ B cells in latency 2 to 3 were characterized by expression of

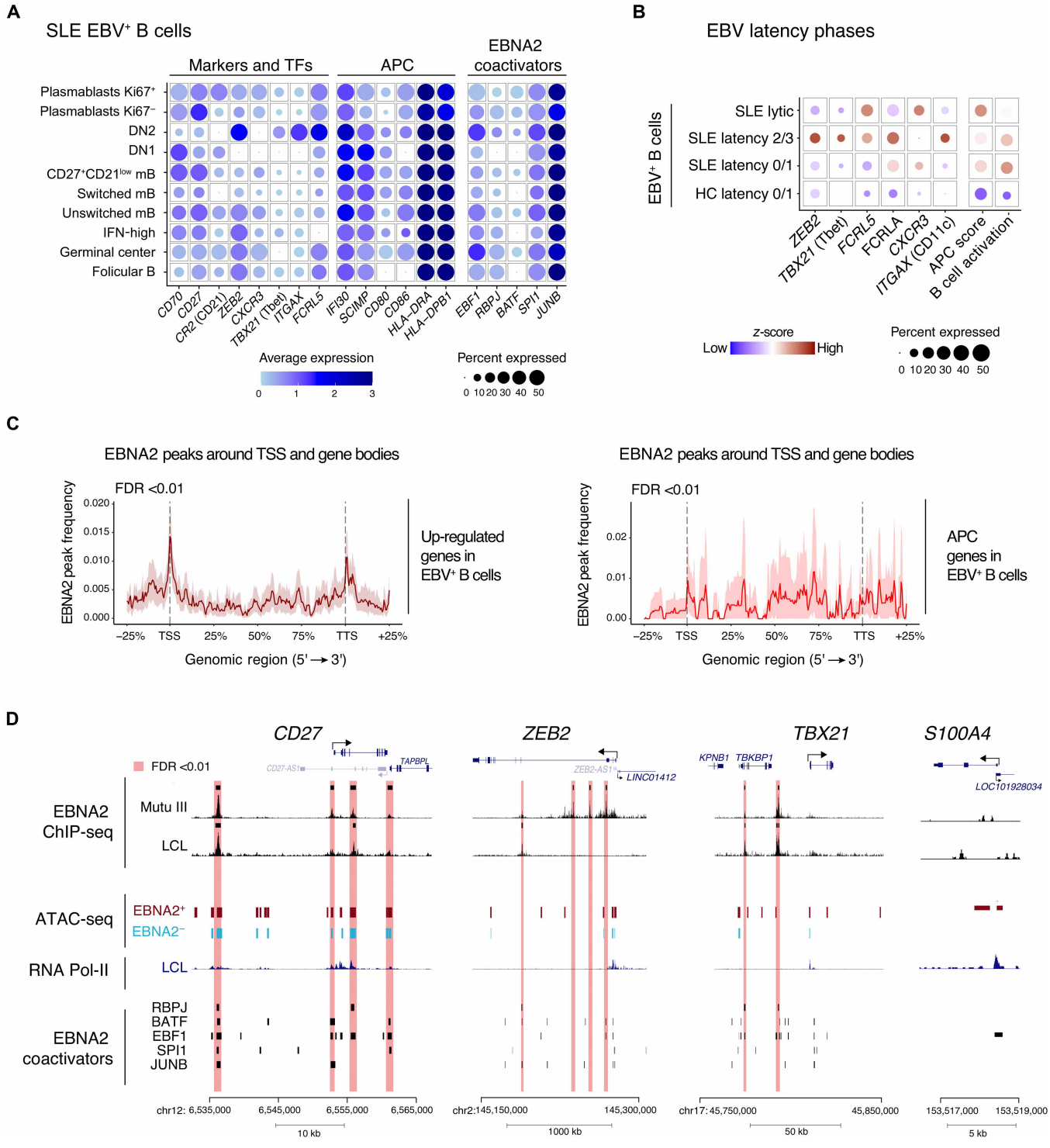

Fig. 5. SLE EBV$^+$ B cells express and EBNA2 binds regions implicated in transcriptional and epigenetic regulation of *CD27*, *ZEB2*, *TBX21* (T-bet), and APC genes in EBV$^+$ B cells from individuals with SLE. (**A**) Expression of B cell markers and TFs in SLE blood EBV$^+$ B cells across B cell subsets. (**B**) Expression of *ZEB2*, *TBX21*, other select markers, and the APC gene module in HC EBV$^+$ B cells in latency 0 to 1 and in SLE EBV$^+$ B cells in latency 0 to 1, latency 2 to 3, or expressing lytic genes. (**C**) EBNA2 ChIP-seq peak density at TSS regions and gene bodies of all up-regulated genes (left) and up-regulated genes related to antigen presentation (right) in SLE EBV$^+$ versus EBV$^-$ CD27$^+$CD21^{low} memory B cells. Histograms show EBNA2 peak frequency (FDR of <0.01) across genomic regions. (**D**) Integrative genomic analysis of ChIP-seq, ATAC-seq, and RNA polymerase II (Pol-II) occupancy data from EBV$^+$ B cell lines (Mutu III and GM12878 LCL) for EBNA2, focusing on the genes encoding CD27 and the TFs Zeb2 and T-bet (*TBX21*), which are up-regulated in EBV$^+$ B cells as shown in (A) and (B) and implicated in SLE pathogenesis. Highlighted red regions indicate EBNA2 binding (FDR of <0.01).

CD27, *ZEB2*, *TBX21*, *FCRL5*, *ITGAX* (CD11c), and APC-related genes (Fig. 5B).

To further define the potential role of EBNA2 in EBV$^+$ B cells in SLE, we integrated our EBV-seq data with previously generated EBNA2 chromatin immunoprecipitation sequencing (ChIP-seq) data (*38*, *39*) and identified ChIP-seq peaks corresponding to EBNA2 binding sites [false discovery rate (FDR) <0.01]. We found that EBNA2 binding was enriched at transcription start site (TSS) regions of the up-regulated genes and APC genes detected in EBV$^+$ CD27$^+$CD21^{low} memory B cells ($P < 0.05$, by Fisher's exact test; Fig. 5C and figs. S6, A and B), suggesting that EBNA2 promotes the activation and expression of APC pathways in EBV$^+$ B cells in SLE.

We next performed integrative genomic analysis combining EBNA2 and coactivator ChIP-seq, assay for transposase-accessible chromatin sequencing (ATAC-seq), and RNA polymerase II occupancy data from multiple EBV$^+$ B cell lines (*22*, *40*–*43*). The identified EBNA2 binding sites localized to upstream enhancer elements at the *CD27* and *CD70* loci and to intragenic or intergenic regions near *ZEB2* and *TBX21* (Fig. 5D and fig. S6C), suggesting that EBNA2 engages both canonical and noncanonical cis-regulatory elements. These EBNA2 binding sites exhibited substantial overlap with previously defined EBV host transcriptional coactivators including recombination signal binding protein for immunoglobulin kappa J region (RBPJ), basic leucine zipper ATF-like transcription factor (BATF), EBV transcription factor 1 (EBF1), serial peripheral interface-1 proto-oncogene (SPI1), and Jun B proto-oncogene (JUNB) (fig. S6).

Analysis of ATAC-seq data identified regions bound by EBNA2 that exhibited increased chromatin accessibility and were enriched in enhancer-associated regions, consistent with EBNA2 functioning as a chromatin-opening transcriptional activator. ChIP-seq profiling of RNA polymerase II revealed transcriptional engagement at these EBNA2-regulated loci. We detected RNA polymerase II occupancy at the TSSs of *CD27*, *CD70*, *ZEB2*, and *TBX21*, with peak intensity aligning with EBNA2-bound and ATAC-accessible regions (Fig. 5D and fig. S6C). Together, these data suggest that EBNA2 cooperatively engages host transcriptional coactivators and epigenetic mechanisms to drive reprogramming of gene expression, thereby promoting the survival, activation, and APC activity of EBV$^+$ cells in SLE.

SLE EBV$^+$ B cells are predominantly singletons and encode antinuclear antigen BCRs

The specificity of the antibodies encoded by EBV$^+$ B cells is unknown. To investigate the reactivity of EBV$^+$ B cells in patients with SLE and HCs, we performed BCR repertoire sequencing (Fig. 6A and fig. S7). SLE EBV$^+$ B cells were predominantly singletons, as compared with EBV$^-$ B cells (Fig. 6B). SLE EBV$^+$ B cells included CD27$^+$IgD$^-$IgM$^+$ as well as isotype-switched CD27$^+$IgD$^-$IgA$^+$ and CD27$^+$IgD$^-$IgG$^+$ memory B cells (Fig. 6C and fig. S8), indicating that the majority of EBV$^+$ B cells in SLE are class switched. We expressed recombinant monoclonal antibodies (mAbs) encoded by SLE EBV$^+$ B cells and demonstrated that they bound HEp-2 cells by immunostaining (Fig. 6D). To determine whether similar findings are present in early SLE, we used EBV-seq to sequence EBV$^+$ B cells from patients with early SLE before receipt of disease-modifying therapy. In recent-onset SLE, EBV$^+$ B cells were also predominantly CD27$^+$CD21^{low} memory B cells that encode antinuclear BCRs (figs. S9 and S10).

SLE EBV$^+$ B cells are members of clonal families that include expanded, affinity-matured EBV$^-$ B cells that encode antinuclear antigen BCRs

B cell repertoire analysis identified EBV$^+$ B cells that were members of clonal families that included expanded EBV$^-$ B cells (EBV$^+$ clonal families; Fig. 6E), with clonal families defined on the basis of shared heavy and light chain V and J gene usage, identical heavy chain complementarity determining region (CDR) 3 lengths, and shared junction sequence similarities as defined by a maximum distance threshold of 0.25 [same V(D)J rearrangement]. These expanded EBV$^-$ B cells (in EBV$^+$ clonal families) were predominantly activated CD27$^+$CD21^{low} memory B cells, DN2 B cells, and plasmablasts (Fig. 6E and figs. S11 and S12). These cells also exhibited higher frequencies of somatic hypermutation and decreased activation and APC scores as compared with their EBV$^+$ B cell family members (Fig. 6E and fig. S12).

We expressed recombinant mAbs from EBV$^+$ clonal families, including from their EBV$^+$ and EBV$^-$ B cell clonal family members, and identified families encoding mAbs that stained the nuclei of HEp-2 cells and bound a spectrum of nuclear antigens, including Smith (Sm) (Fig. 6E). Using biolayer interferometry to measure binding affinity, we demonstrated that the anti-Sm mAbs from the more heavily somatically hypermutated EBV$^-$ B cells bound Sm with higher affinity, as compared with mAbs from their EBV$^+$ B cell clonal family member counterparts ($P < 0.05$, by Student's t test; Fig. 6F). Together, these data demonstrate that SLE EBV$^+$ B cell clonal families can encode autoreactive BCRs and antinuclear antibodies (ANAs) and that the increased somatic hypermutation observed in the EBV$^-$ clonal family member BCRs conferred higher autoantigen binding affinities.

EBV$^-$-related clonal family B cells encode antinuclear antigen BCRs

Analysis of SLE B cell repertoires revealed expanded EBV$^-$ B cells that shared V and J gene usage with their related EBV$^+$ B cell but encoded different V(D)J rearrangements on the basis of the criteria to define clonal families and thus were derived from different progenitor B cells (we term these "EBV$^+$-related families"; Fig. 6G and fig. S13). These expanded EBV$^-$-related B cells (in EBV$^+$-related families) included CD27$^+$CD21^{low} memory and DN2 B cells and exhibited decreased APC scores as compared with their related EBV$^+$ B cells (figs. S12 and S13). Furthermore, mAbs encoded by EBV$^-$-related family members of antinuclear antigen–encoding EBV$^+$ B cells also bound the nuclei of HEp-2 cells (Fig. 6G and fig. S13). We identified EBV$^+$-related families encoding mAbs that bound Sm, and the EBV$^-$ B cells from these related families were more heavily somatically hypermutated and encoded mAbs that bound Sm with higher affinity as compared with their EBV$^+$ family member counterparts ($P < 0.01$; Fig. 6H and figs. S12 and S13). These data suggest that EBV$^+$ B cells also promote activation and affinity maturation of nonclonally related EBV$^-$ B cells that bind the same nuclear autoantigen target. These findings led us to hypothesize that EBV$^+$ antinuclear antigen–encoding B cells are "driver" B cells that serve as professional APCs to activate T helper cells, which in turn provide help to activate related EBV$^-$ B cells encoding antinuclear antigen BCRs.

SLE EBV$^+$ B cells encode antinuclear antigen BCRs that exhibit prototypical ANA staining patterns and antigen binding

We expressed mAbs derived from BCRs expressed by 69 SLE EBV$^+$ B cells, 15 multiple sclerosis EBV$^+$ B cells, and 10 HC EBV$^+$ B cells and characterized them for reactivity to HEp-2 cells using immunostaining

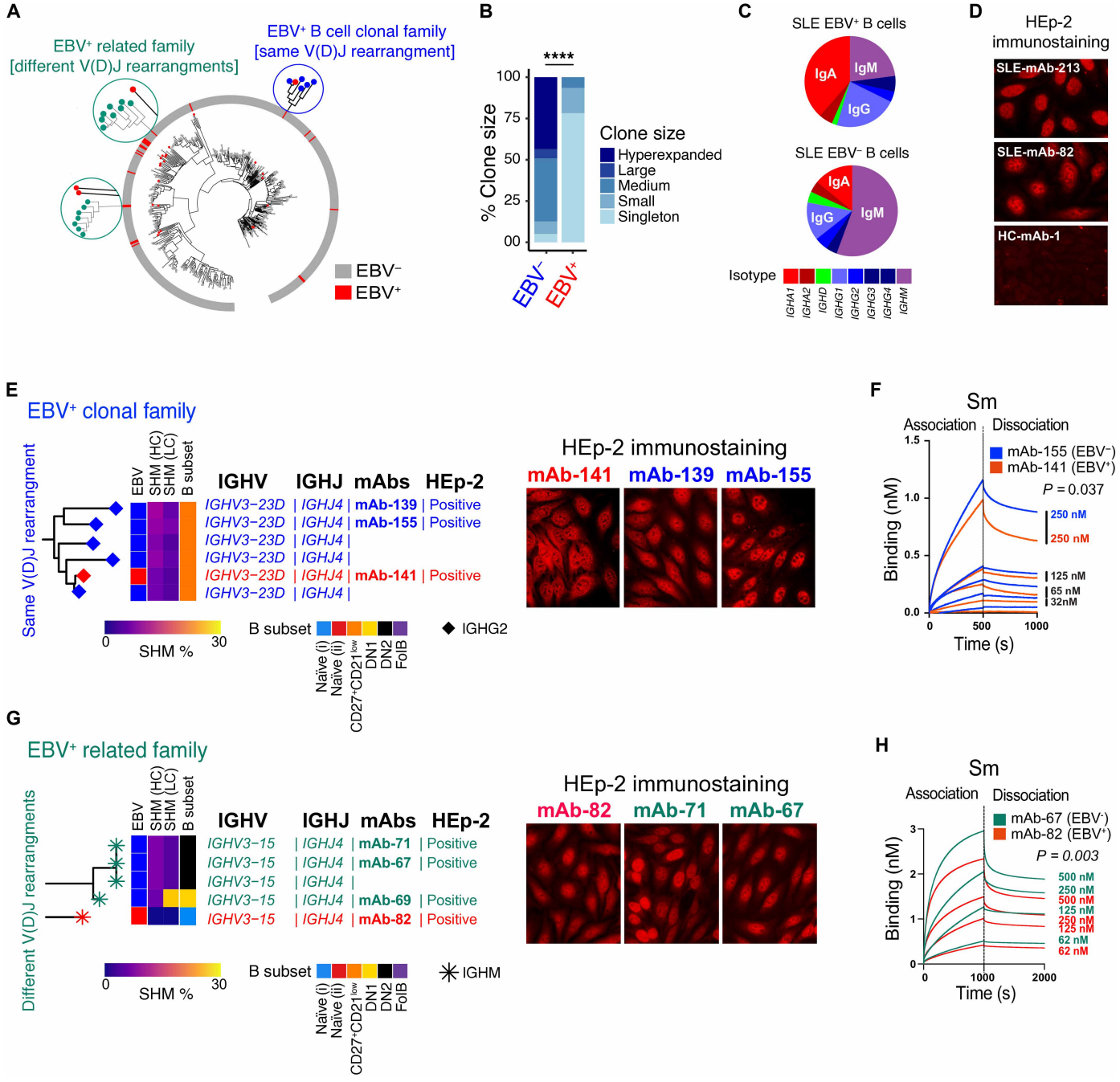

Fig. 6. SLE EBV$^+$ B cells, their clonal family EBV$^-$ B cells, and their related family EBV$^-$ B cells encode antinuclear BCRs. (**A**) Representative phylogenetic tree of *IGHV* genes expressed by SLE blood EBV$^+$ and EBV$^-$ B cells. Examples of EBV$^+$ B cells and their clonal family EBV$^-$ B cells that use the same V(D)J rearrangement indicative of a shared progenitor B cell (dark blue) or their related family EBV$^-$ B cells that use different V(D)J rearrangements indicative of different progenitor B cells (teal). (**B**) Distribution of SLE EBV$^-$ and EBV$^+$ B cell clonal family sizes. For the EBV$^-$ B cells, only the EBV$^-$ B cells in EBV$^+$ B cell clonal families were included. ****$P < 0.0001$, by chi-square test. (**C**) SLE EBV$^+$ and EBV$^-$ B cell immunoglobulin isotype usage. (**D**) SLE and HC EBV$^+$ B cell–derived mAb immunostaining of HEp-2 cells. (**E**) BCR profiles, cell type and somatic hypermutation (SHM), and HEp-2 staining of SLE EBV$^+$ clonal family B cells encoding anti-Sm antibodies. The left schematic shows a clonal family with the same V(D)J rearrangement; node color indicates EBV status of the cells (red, EBV$^+$; blue, EBV$^-$). (**F**) Binding affinity analysis of EBV$^+$ and EBV$^-$ B cell mAbs from the SLE EBV$^+$ clonal family for Sm. (**G**) BCR profiles, properties, and HEp-2 staining of SLE EBV$^+$–related family B cells encoding anti-Sm antibodies. (**H**) Binding affinity analysis of EBV$^+$ and EBV$^-$ B cell mAbs from the SLE EBV$^+$–related family for Sm. For (F) and (H), $P < 0.01$ by Student's *t* test.

and to prototypical SLE antigens using enzyme-linked immunosorbent assay (ELISA). Of 69 SLE EBV$^+$ B cell mAbs, 44 (64%) bound HEp-2 cells (Fig. 7, A and B). In contrast, none of the 10 HC or 15 multiple sclerosis EBV$^+$ B cell mAbs bound HEp-2 cells or SLE-relevant antigens. HEp-2–reactive SLE EBV$^+$ B cell mAbs were derived from multiple B cell subsets, including EBV$^+$ naïve (i), CD27$^+$CD21^{low} memory B cells, DN1 B cells, DN2 B cells, Ki67$^-$ plasmablasts, and Ki67$^+$ plasmablasts (Fig. 7C). They exhibited distinct staining patterns, including nuclear speckled, nuclear homogenous, nucleolar, mixed (nuclear and cytoplasmic), nuclear rim, or DNA and mitotic (Fig. 7A), consistent with the well-defined staining patterns of ANA in SLE. Using ELISA, we identified EBV$^+$ B cells that encoded mAbs that bound

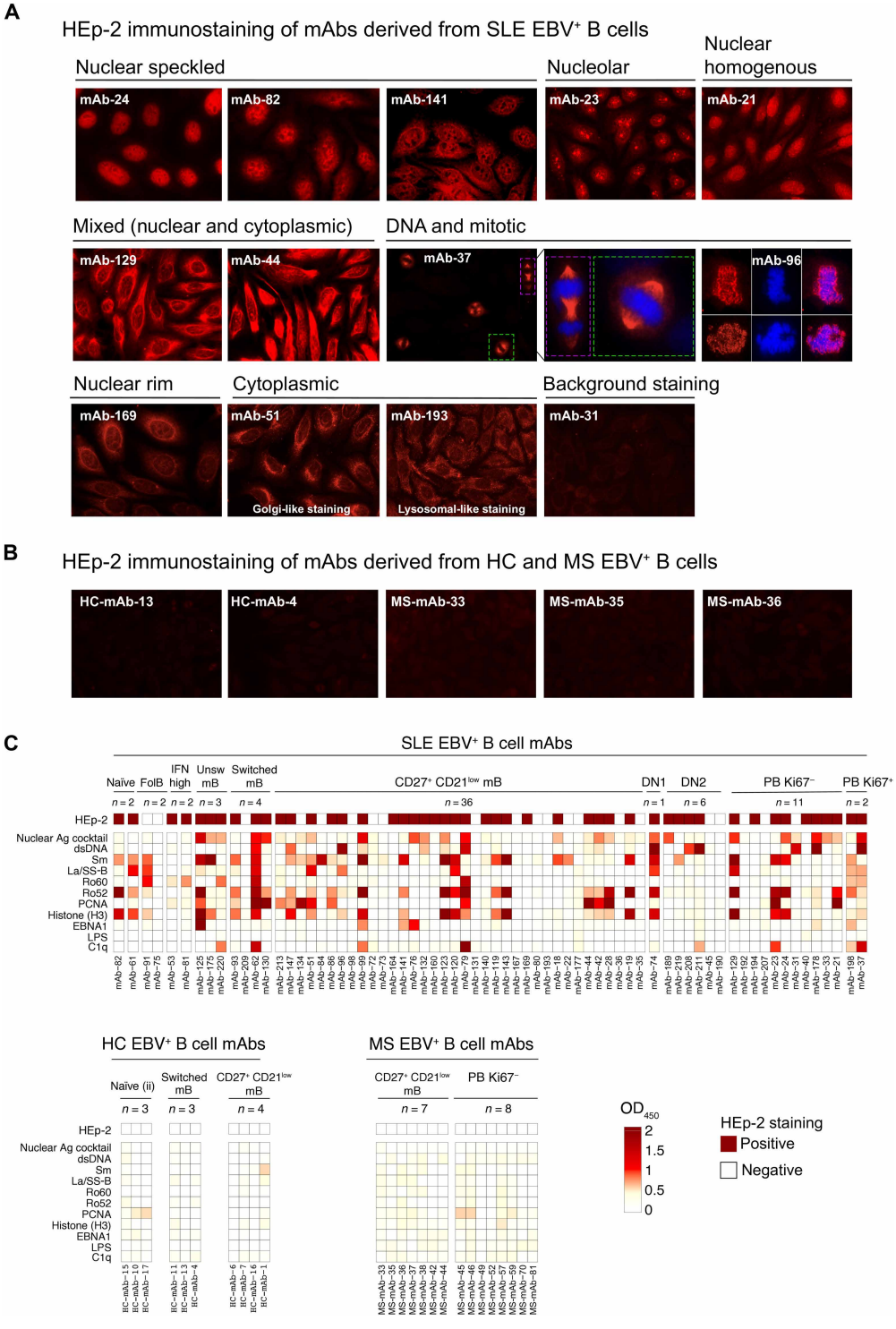

Fig. 7. SLE EBV$^+$ B cell mAb HEp-2 cell immunostaining patterns and their reactivity to prototypical SLE autoantigens. (**A**) Representative examples of immunostaining patterns of SLE EBV$^+$ B cell–derived mAbs on HEp-2 cells. Nuclear homogenous includes both homogenous and fine speckled staining patterns. (**B**) Representative examples of immunostaining of HC and multiple sclerosis (MS) EBV$^+$ B cell–derived mAbs on HEp-2 cells. (**C**) ELISA analysis of the reactivity of SLE, HC, and MS EBV$^+$ B cell–derived mAbs to prototypical SLE autoantigens, including the ANA screen ELISA [nuclear antigen (Ag) cocktail] and individual nuclear antigens, and for EBV EBNA1. As an assessment for potential polyreactive antibodies, LPS ELISAs were performed. The nuclear antigen cocktail, comprising Sm, RNP/Sm, Scl-70, SS-A (Ro) (52 and 60 kDa), SS-B (La), Jo-1, U1-SmRNP, CENP-B, dsDNA, histones, and C1q, was obtained from a commercial source different from that used for the individual antigens in the heatmap. *n*, number of mAbs tested per group; mB, memory B cell.

prototypical SLE nuclear autoantigens including Sm, dsDNA, Ro52, Ro60, histone H3, and proliferating cell nuclear antigen (PCNA), as well as EBV EBNA1 (Fig. 7C). These findings demonstrate that, in SLE, EBV infects autoreactive antinuclear antigen B cells, that SLE EBV$^+$ antinuclear antigen B cells span multiple B cell subsets, and that some SLE EBV$^+$ B cell mAbs can cross-bind EBNA1 and nuclear antigens including Sm.

SLE EBV$^+$ B cell antigen presentation induces activation of T peripheral helper along with antinuclear antigen DN2 B cells

Our EBV-seq results revealed an increase in APC activity within EBV$^+$ B cells in SLE. To evaluate the potential for EBV$^+$ B cells to serve as APCs, we used EBV-transformed lymphoblastoid B cell lines (LCLs) as a model system because of the low frequencies and lack of robust surface markers for EBV$^+$ B cells in blood samples from patients with SLE. LCL B cells represent a latent stage of EBV infection and were previously demonstrated to function as APCs (*44*, *45*). To investigate the potential role of EBV$^+$ B cells as APCs in SLE, we generated EBV$^+$ LCLs using samples from patients with SLE who had serum anti-DNA autoantibodies on the basis of clinical laboratory test results. LCLs were loaded with chromatin complexes using an avidin-conjugated anti-DNA mAb combined with biotinylated anti-IgM/G antibodies (Fig. 8A), based on previously described methods to load B cells with extracellular chromatin present in culture medium (released from dying cells) (*46*).

Chromatin-loaded SLE LCLs were cultured with isolated T and B cells from the same MHC-matched patients with anti-DNA autoantibody–positive SLE; after 10 days, cultured cells were collected for scRNA-seq and supernatants for HEp-2 immunostaining (Fig. 8A). scRNA-seq analysis demonstrated expansions of CD4$^+$PD1^{hi}CXCR5$^-$ (PD1, programmed cell death protein 1) T peripheral helper (T_{PH}) cells (*47*) ($P < 0.0001$; Fig. 8B and figs. S14 and S15) and expansions of EBV$^-$ DN2 B cells (non-LCLs) (****$P < 0.0001$; Fig. 8C and figs. S14 and S15). Recombinant mAbs were generated from clonally expanded B cells (shared heavy and light chain V and J gene usage, identical heavy chain CDR3 lengths, and shared junction sequence similarities as defined by a maximum distance threshold of 0.25) and tested for immunostaining of HEp-2 cells. We identified multiple clonally expanded EBV$^-$ DN2 and EBV$^-$ plasmablast B cells that encoded mAbs that bound HEp-2 cells, demonstrating that these B cells are autoreactive and can produce ANAs (Fig. 8D).

We further tested culture supernatants for antibodies that stain HEp-2 cells. Culture supernatants from chromatin-loaded SLE LCLs cultured with T and B cells from the same patients with anti-DNA autoantibody–positive SLE contained increased ANAs that bound HEp-2 cells as compared with cultures with MHC-mismatched T and B cells from different patients or with chromatin-loaded HC LCLs (****$P < 0.0001$, by Student's t test; Fig. 8E). Together, these results demonstrate that SLE EBV$^+$ LCLs can serve as APCs to mediate activation of T_{PH} cells along with EBV$^-$ autoreactive antinuclear antigen DN2 B cells and plasmablasts.

DISCUSSION

More than 94% of the human population is infected with EBV, whereas only a small proportion of these individuals develop SLE. Here, using EBV-seq, we demonstrated that EBV directly infects autoreactive antinuclear antigen B cells in the peripheral blood of patients with SLE and reprograms them as activated APCs. In contrast, HC EBV$^+$ B cells did not encode antinuclear antigen BCRs and exhibited fewer features associated with antigen presentation. Integrative analyses of ChIP-seq, ATAC-seq, and RNA polymerase II occupancy data revealed that EBNA2 may mediate both transcriptional and epigenetic regulation of *CD27*, *CD70*, *ZEB2*, *TBX21*, and genes associated with antigen presentation through direct binding to their regulatory elements and recruitment of host TFs, including coactivators such as RBPJ. SLE EBV$^+$ B cells in latency 3, the latency phase in which EBNA2 is expressed, exhibited increased expression of these genes. We showed in vitro that EBV$^+$ B cell–mediated presentation of prototypical SLE antigens as chromatin was sufficient to induce the activation of autoreactive T and antinuclear antigen B cell responses, including EBV$^-$ antinuclear antigen B cells. In contrast, HC EBV$^+$ B cells did not encode antinuclear antigen BCRs, were less able to function as APCs, and did not induce ANA responses. Together, our data demonstrate that EBV infection reprograms antinuclear antigen B cells as activated APCs and that EBV$^+$ autoreactive B cells have the potential to serve as "driver" B cells that orchestrate activation of systemic autoimmune responses that mediate the pathogenesis of SLE.

Our findings provide a mechanistic basis for why only a small fraction of EBV-infected individuals develop SLE whereby EBV infects autoreactive antinuclear antigen B cells, which are known to be present in the naïve B cell compartments of patients with autoimmune diseases but not healthy individuals (*48*). We showed that patients with SLE have more than 20-fold higher numbers of EBV$^+$ B cells as compared with HCs, suggesting a potential central role for these cells in the pathogenesis of SLE. Several mechanisms may contribute to this expansion, including deficient anti-EBV CD8 T cell responses (*8*, *49*, *50*), EBV-mediated immune evasion (*1*, *8*), infection with an EBV strain that promotes B cell survival or growth (*21*), therapeutic immunosuppression allowing expansion of EBV$^+$ B cells, host-pathogen interactions that accelerate disease progression, or other mechanisms.

In SLE, EBV$^+$ B cells were predominantly detected within the CD27$^+$CD21^{low} memory B cell subset and express *ZEB2* and *TBX21*. EBV infects naïve B cells through CD21 (*51*, *52*), and our trajectory analysis suggests that EBV$^+$ naïve, DN2, and follicular B cells all differentiate toward EBV$^+$ CD27$^+$ CD21^{low} memory B cells, which can be subsequently stimulated to differentiate into plasmablasts. SLE EBV$^+$ CD27$^+$CD21^{low} memory B cells exhibited increased expression of the gene encoding CD70, the ligand for CD27, which might contribute to EBV$^+$ B cell activation and survival in SLE. CD70 is a marker of mature B cells recently primed by antigen and capable of producing high-affinity antibodies upon T cell–dependent stimulation (*31*).

Integrative analysis of ChIP-seq, ATAC-seq, and RNA polymerase II occupancy data revealed EBNA2 binding at the transcriptional start sites and regulatory regions of *CD27*, *CD70*, *ZEB2*, and *TBX21*. These findings provide a molecular basis by which EBV may directly promote the development of CD27$^+$CD21^{low}ZEB2$^+$ T-bet$^+$ activated memory B cells with APC function. Consistent with this potential mechanism, EBV-infected LCLs showed up-regulation of *CD27*, *CD70*, and other APC-related genes. Together, these results support a model in which EBV infection, through EBNA2-mediated epigenetic and transcriptional remodeling, can reprogram autoreactive antinuclear antigen B cells into pathogenic "driver" APCs in SLE.

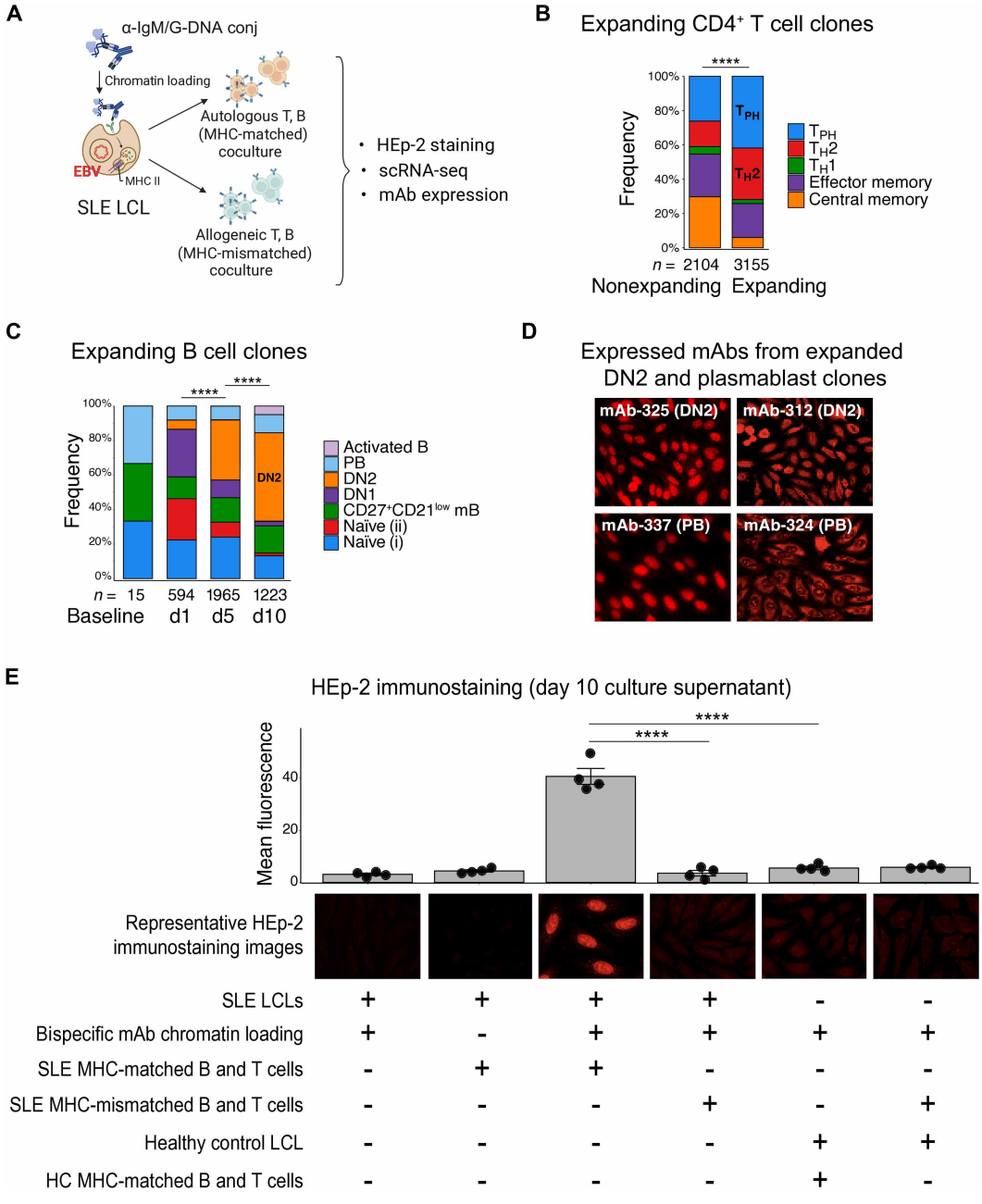

Fig. 8. SLE EBV$^+$ LCLs serve as APCs that promote expansion of T_{PH} and EBV$^-$ ANA-encoding DN2 B cells and plasmablasts. (**A**) Schematic overview of LCL cocultures with T and B cells. LCLs were generated from patients with SLE who have anti-DNA autoantibodies. SLE LCLs were loaded with chromatin using a combination of anti-IgG/M-avidin and anti–DNA-biotin antibodies (free chromatin is present in culture supernatants because of low amounts of dying cells). Chromatin-loaded LCLs were washed and then cocultured with T and B from the same patient (SLE MHC–matched B and T cells), or from a different patient with anti-DNA autoantibodies (SLE MHC–mismatched B and T cells). HC LCLs, as well as T and B cells, were used as controls. (**B**) Frequency of T cell subsets, including PD1^{hi}CXCR5$^-$CD4$^+$ T_{PH} cells, at day 10 among nonexpanding and expanding CD4$^+$ T cell clones as measured by scRNA-seq. ****$P < 0.0001$, by chi-square test. (**C**) Frequencies of the B cell subsets among the expanded EBV$^-$ SLE B cells as measured by scRNA-seq. ****$P < 0.0001$, by chi-square test. (**D**) Immunostaining of HEp-2 cells with expressed mAbs from expanded DN2 B cell and plasmablast clones in coculture from (C). (**E**) Immunostaining of HEp-2 cells using culture supernatants collected at day 10. The top bar graph presents the mean fluorescence of HEp-2 staining, with the values representing the average pixel intensity within a selected region of interest measured by ImageJ. Data are shown as means ± SEM. ****$P < 0.0001$, by Student's *t* test. d, day; T_H, T helper.

Prior studies reported key roles for autoreactive T_{PH} (*47*, *53*) and antinuclear antigen DN2 B cells and plasmablasts in SLE (*16*, *17*), yet how autoreactive T_{PH} and autoreactive DN2 B cells become activated has been an open question (*47*, *53*). The fact that antinuclear antigen EBV^+ B cells belong to the same clonal family as other antinuclear antigen EBV^- B cells suggests that EBV infection occurred during an ongoing autoimmune response. In agreement with this scenario, the main EBV^+ B cell fraction in samples from patients with SLE consists of $CD27^+CD21^{low}$ memory B cells, which were previously identified as activated memory B cells that arise after a germinal center response (*11*–*13*). However, autoimmune responses in SLE may rather involve extrafollicular B cell responses (*17*, *53*, *54*). This apparent discrepancy may be explained by our observation that some EBV^+ B cells in SLE express BCRs that recognized EBV EBNA1 and cross-reacted with Sm or other nuclear antigens. Hence, EBV may directly infect anti-EBNA1 B cells with autoimmune cross-reactivity in SLE (as well as infect other autoreactive antinuclear antigen B cells), which may then serve as APCs and enhance and orchestrate the pathogenic autoimmune response in SLE through antigen-specific activation of T_{PH} cells. Activated T_{PH} cells may further activate related EBV^- B cell clones and other autoreactive B cells that recognize similar self-antigens and provide them proliferative and differentiation signals that allow them to develop into DN2 B cells and plasmablasts. As a consequence, EBV^--related B cell clones display increased frequencies of somatic hypermutation and ANA affinity compared with those of EBV^+ B cells, and the secretion of these ANAs contributes to SLE pathology. This could promote the previously described EBNA1-Sm molecular mimicry in SLE (*18*, *19*).

In healthy individuals, ~20% of mature naïve B cells emerging from the bone marrow encode antibodies with HEp-2 reactivity, and peripheral tolerance checkpoints typically limit the survival and activation of these autoreactive clones (*55*). EBV has been shown to impair peripheral tolerance (*24*, *41*, *56*). Our data suggest that, in SLE, EBV infection promotes the survival and activation of autoreactive EBV^+ antinuclear antigen B cells by overcoming these checkpoints. Moreover, our observation of expanded clonally related EBV^- antinuclear antigen B cells suggests that intrinsic defects in peripheral tolerance, independent of EBV, also play a role in the development of autoreactive clones in SLE.

Using groups of EBV genes associated with distinct latency phases, we were able to classify SLE EBV^+ B cells into latency 0 to 1, latency 2 to 3, and lytic phases and demonstrated that SLE EBV^+ B cells in latency 3 exhibited up-regulation of *ZEB2*, *TBX21*, and antigen presentation genes. EBNA2 expression is specifically associated with latency 3 (*1*), and, although we also observed elevated antigen presentation gene expression in SLE EBV^+ B cells in 0 to 1, suggesting that EBV^+ B cells in latency 0 to 1 may promote antinuclear autoimmunity in SLE, development of EBV^+ B cells in latency 3 may further promote antinuclear autoimmunity in SLE. The extent to which EBV^+ B cells in different subsets and latency states mediate activation of broad antinuclear antigen T_{PH} cell and antinuclear antigen EBV^- B cell responses in SLE remains an important area for further investigation.

Lytic reactivation has been associated with disease onset and flares in SLE (*3*); however, it remains unclear whether EBV reactivation drives autoimmune flares or is instead triggered by them. In this study, we showed that EBV^+ B cells in SLE are predominantly $CD27^+CD21^{low}$ memory B cells in latency yet exhibit transcriptional features of activated APCs. In addition, we detected small populations of EBV^+ naïve B cells, memory B cells, DN1 B cells, DN2 B cells, and plasmablasts expressing lytic reactivation genes in samples from patients with SLE but not in HCs. These findings suggest dynamic reactivation of EBV in SLE, which may involve both the abortive lytic cycle and overt lytic reactivation (*27*). Differentiation of memory B cells into plasmablasts is known to induce expression of the plasma cell TFs X-box binding protein 1 (XBP-1) and B lymphocyte–induced maturation protein 1 (BLIMP-1), which can directly activate the EBV immediate-early gene BamHI Z Epstein-Barr virus replication activator (BZLF1) and thereby trigger lytic reactivation (*57*). Therefore, it is possible that some of the lytic-phase EBV gene expression we observed, particularly in plasmablasts, reflects a bystander consequence of inflammatory B cell differentiation rather than a driver of disease activity.

By which mechanisms is EBV infection contributing to B cell–mediated autoimmunity? Our results revealed enrichment of EBNA2 binding near the transcriptional start sites of ZEB2, TBX21, genes associated with APC function, and other genes up-regulated in EBV^+ B cells from patients with SLE. These findings suggest that EBNA2-host interactions mediate transcriptional reprogramming of autoreactive antinuclear antigen B cells, promoting their differentiation into pathogenic "driver" APCs. In addition to EBNA2, EBV has also been demonstrated to promote B cell activation through multiple latency-associated mechanisms, including EBER-mediated Toll-like receptor 3 (TLR3) activation (*58*); EBV BamHI-A rightward transcript (BART) microRNA activation of nuclear factor κB and extracellular signal-regulated kinase 1/2 (Erk1/2) (*59*); EBNA1-promoted B cell survival (*3*, *60*); and other mechanisms (*1*, *23*, *24*, *41*). In latency 2, latency 3, and during lytic reactivation, EBV may further promote activation of autoreactive antinuclear antigen B cells through additional mechanisms. These include expression of LMP1, a constitutively active CD40 mimic, and LMP2A, a functional homolog of the BCR (*1*, *22*, *23*). Together, these viral proteins can drive up-regulation of costimulatory molecules on B cells, thereby enhancing the ability of autoreactive antinuclear antigen EBV^+ B cells to interact with and activate autoreactive T cells.

Although peripheral B cell depletion with the anti-CD20 mAb rituximab did not demonstrate efficacy in randomized controlled trials in SLE or lupus nephritis (*61*), recent pilot trials suggest that CD19–chimeric antigen receptor (CAR) T cell–mediated and potentially anti-BCMA T cell engager bispecific antibody-mediated ultra-deep B cell depletion of both peripheral and tissue B cells can provide dramatic clinical benefit and long-term remission (*62*, *63*). An intriguing hypothesis is that the durability of the efficacy of CD19–CAR T cell and anti-BCMA T cell engager bispecific antibody therapy in SLE arises from the depletion of EBV^+ antinuclear antigen driver B cells. Further investigation is needed to determine whether solely depleting EBV^+ B cells will provide efficacy in established SLE or whether depletion of EBV^- antinuclear antigen DN2 B cells, plasmablasts, or other B cells is also necessary to effectively treat ongoing autoimmunity.

EBV infection and reactivation are also associated with other autoimmune diseases, including multiple sclerosis, Sjögren's syndrome, and rheumatoid arthritis; EBV reactivation has also been linked to Long Covid (*21*). It is possible that EBV infection and reprogramming of autoreactive B cells as driver APCs could play a central role in these autoimmune conditions and potentially others.

Our study has some limitations. Because of technical limitations of EBV-seq in detecting low-abundance viral transcripts, we were

limited in our ability to classify EBV$^+$ B cells by latency or lytic phase. Another limitation was the use of frozen instead of fresh peripheral blood mononuclear cells (PBMCs), because freezing can affect transcriptomic results and might also affect EBV gene expression or other aspects of EBV infection. Last, patients with SLE exhibit impaired CD8 T cell responses to EBV (*8*, *49*, *50*), and immunosuppressive therapy is associated with increased EBV reactivation (*64*). In this study, immunosuppressive therapy may have reduced immune control of EBV, thereby contributing to both increased EBV$^+$ B cell frequencies and the increased expression of EBV reactivation genes.

In summary, we provide evidence that, in SLE, EBV infects and reprograms autoreactive antinuclear antigen B cells, which then have the potential to serve as driver APCs capable of activating antinuclear T and EBV$^-$ B cell responses that promote disease. Our findings provide a potential mechanistic basis for the role of EBV in the initiation and persistence of autoimmunity in SLE. This framework may also be relevant to other EBV-associated autoimmune conditions.

MATERIALS AND METHODS

Study design

SLE and healthy comparator peripheral blood samples were collected at Stanford University. SLE was diagnosed based on the Systemic Lupus International Collaborating Clinics (SLICC) classification criteria. All patients with SLE and HC individuals were EBV$^+$, as assessed by elevated anti-EBNA1 antibody titers. Demographic and clinical data were collected for each patient, and none of the patients had received anti-CD20 or other B cell depletion therapy prior to the time of sample collection (table S2). The sample size used is in line with our prior scRNA-seq BCR repertoire studies. Human participant sample collection was approved by the Stanford University Institutional Review Board (protocol 3470), and written informed consent was obtained from all patients and HC participants.

PBMC isolation and B cell enrichment

PBMCs were isolated using density gradient centrifugation using Ficoll-Paque PLUS (GE Healthcare). The isolated PBMCs were cryopreserved in Recovery Cell Culture Freezing Medium (Gibco) at a concentration of 10 million cells/ml. To remove dead cells, thawed PBMCs were processed using the EasySep Dead Cell Removal (Annexin V) Kit (STEMCELL Technologies) according to the manufacturer's instructions. Viable cells were subjected to magnetic bead–based B cell isolation using the EasySep Human B Cell Isolation Kit (STEMCELL Technologies) according to the manufacturer's instructions. Through this procedure, non–B cells were depleted using tetrameric antibody complexes and magnetic particles, resulting in a >95% pure B cell population for scRNA-seq.

EBV-specific primers for EBV-seq

To enable high-throughput scRNA-seq of a panel of EBV genes, we developed an extension to the 10x Genomics 5′ RNA-seq platform, in which 23 primers specific for 21 EBV genes were added in during reverse transcription and amplification PCRs (Fig. 1, A and B, and table S1). These primers included a 22–base pair (bp) handle 5′-AGCAAGTGAGAAGCATCGTGTC-3′ and were synthesized as DNA oligonucleotides (Integrated DNA Technologies). During PCR library amplification, we added a reverse EBV-primer to enrich for EBV cDNAs and used the 10x Genomics protocol for library preparations. The barcoded libraries were sequenced using Illumina NovaSeq 6000 (Novogene) to sequence ~700 million reads per sample, and data aligned to the human reference genome GRCh38 using STARsolo (v2.7.9a). Subsequently, reads that did not map to the human genome were aligned to the EBV genome (NC_007605) using STARsolo (v2.7.9a) with the following parameters: --outFilterScoreMinOverLread 0.5 --outFilterMatchNminOverLread 0.5. The UMIs of uniquely mapped reads to EBV genome were counted (EBV gene UMI counts) using HTSeq (v2.0.3). The uniquely mapped EBV gene reads were visualized using Integrative Genomics Viewer (v2.14.1). The matrix of the EBV UMI gene counts was integrated with human gene counts using Seurat package (v.4.9.9). The GTF (gene transfer format) file for EBV annotation (NC_007605) was modified to enhance the annotation of RPMS1 transcript by adding the annotation to three additional exons: exon 2, 139447–139552; exon 3, 140558–140691; and exon 4, 146233–146333.

Evaluation of the range of EBV gene UMI counts demonstrated that B cells with ≥2 EBV gene UMI counts (for any of the EBV genes for which primers were included in EBV-seq, see Fig. 1B and table S1) exhibited increased EBV infection module scores [Kyoto Encyclopedia of Genes and Genomes (KEGG) hsa05169, EBV infection], SLE EBV$^+$ B cell predictor scores, B cell activation scores [Gene Ontology (GO):0042113], APC scores (GO:0019882), and frequencies of somatic hypermutation in the immunoglobulin heavy chain as compared with EBV gene UMI count 0 and 1 B cells (fig. S16). B cells with ≥2 EBV gene UMI counts exhibited similar EBV infection module, SLE EBV$^+$ B cell predictor, B cell activation, and APC scores as compared to EBV gene UMI count 3, 4, or ≥5 B cells (fig. S16). Based on these findings, we selected a threshold of ≥2 EBV gene UMI counts for identifying EBV$^+$ B cells for the analyses presented herein (Figs. 1 to 4 and figs. S2 to S13). In addition, B cells with only 1 EBV gene UMI count were also classified as EBV$^+$ if they belonged to a clonal family that included another B cell with ≥2 EBV gene UMI counts.

EBER–flow cytometry

To analyze EBV$^+$ B cell by EBER–flow cytometry, EBV small RNAs (EBER1/2) were detected using hybridization chain reaction (HCR) RNA–fluorescence in situ hybridization with the HCR Gold Kit (Molecular Instruments). PBMCs were surface stained with anti-human CD19 mAb (clone HIB19, BioLegend, catalog no. 302218; APC/Cy7, 1:50 dilution in fluorescence-activated cell sorting buffer) for 30 min at 4°C in the dark. Following staining, cells were washed three times with phosphate-buffered saline (PBS) supplemented with 2% fetal bovine serum (FBS) and subsequently fixed and permeabilized using the True-Nuclear Transcription Factor Buffer Set (BioLegend, catalog no. 424401) according to the manufacturer's instructions. Cells were then hybridized overnight at 37°C with probe sets targeting EBER1/2. After washes, HCR signal amplification was performed with fluorophore-labeled amplifiers. Cells were analyzed on a Cytek Aurora spectral flow cytometer. Data were processed in FlowJo v10, and EBER1/2$^+$ B cells were quantified as a percentage of total CD19$^+$ B cells.

scRNA-seq with EBV-seq, CITE-seq, and BCR/TCR-seq

For multimodal scRNA-seq, we combined EBV-seq, CITE-seq, BCR-seq, and scRNA-seq using the 10x Genomics 5′ RNA-seq platform to sequence the EBV genes, BCR/T cell receptor (TCR) repertoires,

and transcriptomes of blood B cells from patients with SLE and HCs. For each sample, we started with 10 million frozen PBMCs, performed dead cell removal using the Dead Cell Removal Kit (STEMCELL Technologies) as described above, and isolated untouched B cells using negative selection (STEMCELL Technologies) as described above. In accordance with 10x Genomics protocols, B cells were resuspended at a concentration of 1000 cells/μl, and ~20,000 cells were loaded onto each lane of the 10x Genomics chromium chip.

Computational analysis of scRNA-seq datasets

Sequenced gene expression libraries and V(D)J libraries were demultiplexed, converted into FASTQ files, and mapped to the GRCh38 reference genome using Cell Ranger (v6.0.0) and its default parameters. The gene expression reads were aligned to the human reference sequence GRCh38, and the BCR and TCR V(D)J sequences were annotated using the vdj-GRCh38-alts-ensembl reference database provided by 10x Genomics. CITE-seq sequenced FASTQ files were processed using the CITE-seq-Count package (v1.4.2). Gene expression counts were analyzed using the Seurat package (v.4.9.9), including filtering to remove cells with >10% mitochondrial reads, <250 unique genes, or <1000 UMIs. Doublets were identified using scds R package (v1.20.0) (*65*) and excluded. Samples derived from the same donor were merged and normalized using SCTransform to regress out the percent mitochondrial reads and cell cycle reads (S.Score and G2M.Score). SCTransform identified the top 3000 variable genes in each dataset. Samples were merged into individual Seurat objects and harmonized for batch effects using the Harmony package (v1.2.0) (*66*). Principal components analysis (PCA) was performed using the 3000 variable genes in each dataset, and based on the elbow plot, 40 PCs were selected and input into uniform manifold approximation and projection (UMAP) algorithm for visualization. Clustering was performed using the FindNeighbors (using 40 PCs) and the FindClusters (resolution = 0.5) functions.

Cluster labels were manually adjusted based on DEGs identified with the FindAllMarkers function, which only used genes found in at least 25% of cells in either of the two input comparison groups and only returned results for genes with at least a 0.5 log-transformed fold change between groups. The cluster annotations were made according to the differential expression of canonical B cell lineage markers, and B cell subtypes confirmed by quantification of surface markers using reads representing the CITE-seq antibodies and VDJ-seq–based isotype detection.

Differential gene expression analysis and GO analyses

DEGs between EBV^+ as compared to EBV^- B cells were identified using the Poisson generalized linear model for comparing two independent groups (*67*). Genes were considered for analysis if they met the following criteria: an average $\log_2$ fold change ($\log_2$FC) greater than 0.2, an FDR less than 0.1, and expression in >25% of cells or in at least 10 cells within the EBV^+ group. After filtering, the identified DEGs were input into GO analysis using the clusterProfiler (v4.10.1) package (*68*). Ribosomal and mitochondrial genes were excluded from the DEGs used in GO analyses. The background gene set for GO analysis included all genes expressed in all B cell subsets. TFs and their regulatory interactions were analyzed using the TRRUST database (v2).

Gene scores

We obtained the list of genes for each module from GO database for Antigen Processing and Presentation (GO:0019882) and B cell Activation (GO:0042113). The gene lists were filtered to remove genes not expressed in our datasets (a subset of the genes in the gene sets listed in table S4). The AddModuleScore function infers the activity of the individual gene sets by calculating the average expression of each gene set on a single-cell level, after subtracting the aggregated expression of control feature sets, and was used to identify gene modules. Analyzed features were binned based on averaged expression, and control features randomly selected from each bin using default parameters. Distribution of the scores was compared between the groups (HC, SLE, EBV^+, and EBV^-) for each cluster, and two-sided Wilcoxon rank sum test was used to determine significance.

Trajectory analysis

EBV^+ B cell trajectory analysis was performed using RNA velocity analysis to infer transcriptional dynamics and lineage trajectories across B cell subsets. Spliced and unspliced transcript count matrices were generated from aligned files using velocyto (v0.17.17) with default parameters (*36*). These matrices were imported into scVelo (v0.1.25) in Python for downstream analysis (*37*). The data were normalized and log-transformed, and highly variable genes were selected to ensure robust velocity calculations. RNA velocity was estimated using the scVelo dynamical model, which infers transcriptional dynamics based on splicing kinetics and predicts future cell states and thereby B cell subsets.

BCR and TCR sequence analysis

BCR and TCR region sequences were analyzed using the Cell Ranger pipeline in combination with the Immcantation toolkit (*69*). Raw sequencing data were processed with Cell Ranger (v6.0.0) to generate annotated human BCR and TCR sequences, and the contig annotations imported into the Immcantation (v4.4.0) pipeline. The BCR sequences underwent filtering, and sequences were excluded if they were nonproductive, lacked a heavy chain, or contained multiple heavy chain sequences per single cell. BCR sequences that passed filtering were subjected to clonal partitioning using the scoper R package (v1.3.0) (*70*). The sequences were grouped into clonal families based on shared V-J gene rearrangements, identical CDR3 lengths, and shared junction sequence homology, as defined by a maximum distance threshold of 0.25. Germline sequences were determined based on the assigned V-J genes along with the consensus sequence for each B cell suing the dowser R package (v2.2.0). The germline sequence was used as the reference for calculating the frequencies of somatic hypermutation in both the heavy and light chains. TCRαβ sequences were excluded if they were nonproductive or had multiple beta or alpha chains per single cell. The T cells were grouped into clonal lineages based on their TCR sequences having shared V-J genes and identical CDR3 amino acid sequences.

Phylogenetic tree construction

Phylogenetic relationships among the BCR heavy chain sequences were inferred using the Neighbor-Joining (NJ) method from the phangorn package in R (v2.11.1) (*71*). The distance matrix required for the NJ algorithm was calculated using the maximum likelihood method using phangorn R package. The resulting NJ trees

were visualized and annotated using the ggtree package (v3.10.1) (*72*), and the ggplot2 package (v 3.5.1) was used to incorporate the EBV infection status and BCR information into the tree visualizations.

Selection and expression of recombinant mAbs

Variable heavy and light chain sequences were selected based on (i) being encoded by an EBV^+ B cell, (ii) being a member of EBV^+ B cell clonal family, or (iii) being a member of an EBV^+ B cell–related family (Fig. 4, E and G). For recombinant expression, heavy- and light-chain variable sequences were codon optimized, synthesized (GenScript), and cloned into in-house vectors encoding the human IgG1 heavy chain constant region or κ or λ light chain constant regions, respectively. Both plasmids were transiently transfected into Expi293F cells using FectoPRO (Polyplus, catalog no. 101000014). Supernatants were collected after 7 days, and mAbs were purified with AmMag Protein A magnetic beads (GenScript). Antibody concentrations were measured with a NanoDrop spectrophotometer. Quality control of expressed mAbs was achieved by gel electrophoresis and Coomassie staining.

HEp-2 cell immunostaining

HEp-2 cells, an epithelial cell line derived from HeLa cells, were cultured in Dulbecco's modified Eagle's medium supplemented with 10% FBS and 1% penicillin-streptomycin. When cells reached 70 to 80% confluence, they were harvested using trypsin-EDTA and seeded onto poly-L-lysine–coated eight-well slides. After 24 hours, cells were fixed in 4% paraformaldehyde in PBS for 10 min at room temperature and permeabilized with 0.25% Triton X for 15 min at room temperature. Cells were then washed three times with PBS and blocked with 1% bovine serum albumin (BSA) in PBS for 30 min at room temperature. mAbs were diluted in PBS containing 0.1% BSA to a concentration of 1 to 10 μg/ml, mAbs were added to HEp-2 cells, and cells were incubated for 2 hours at room temperature, followed by three washes with PBS and incubation with Alexa Fluor 594–conjugated anti-human IgG (1 μg/ml in PBS + 1% BSA) for 30 min. Slides were washed again and mounted using 4′,6-diamidino-2-phenylindole (DAPI)–containing mounting medium and imaged using a KEYENCE Microscope.

Enzyme-linked immunosorbent assay

ELISAs were conducted by coating Costar 96-well assay plates (Corning, catalog no. 9018) with 1 μg/ml of each of the antigens: Sm (Surmodics, catalog no. 13301), Ro/SS-A (52 kDa; Surmodics, catalog no. A12701), Ro62 (Surmodics, catalog no. 17401), dsDNA (Sigma-Aldrich, catalog no. 11691112001), La/SS-B (Surmodics, catalog no. A12801), PCNA (Surmodics, catalog no. A15401), histone H3 (Cayman, catalog no. 10263), EBNA1 (Abcam, catalog no. ab138345), or lipopolysaccharide (LPS; Invitrogen, catalog no. 00-4976-93) in carbonate-bicarbonate buffer at 4°C overnight. The plates were washed six times with PBST (PBS + 0.05% Tween 20) and blocked with blocking buffer (Blocker Casein in PBS, Thermo Fisher Scientific, catalog no. 37528) for 1 hour at 37°C. mAbs were diluted in PBS + 0.2% casein and added at a concentration of 10 μg/ml, followed by incubation for 2 hours at room temperature. The plates were washed six times with PBST. Horseradish peroxidase (HRP)–conjugated goat anti human IgG (H+L) secondary antibody (Invitrogen, catalog no. 31410; 1:5000 dilution) was added to each well and incubated at room temperature for 1 hour. After six additional washes with PBST, 3,3′,5,5′-tetramethylbenzidine (TMB) substrate (Thermo Fisher Scientific, catalog no. N301) was added followed by incubation in the dark at room temperature for 15 min. The reactions were stopped with Stop solution (Invitrogen, catalog no. CNB0011), and the optical density (OD) of the solution at 450 nm was read on a BioTek Synergy H1 Multiplate Reader. An ANA negative mAb was run on each ELISA plate as an internal negative control to account for plate-to-plate background variability. The final OD_{450} values were normalized by subtracting the negative control mAb OD_{450} values from each of the tested mAbs OD_{450} values. Background subtracted OD_{450} values were visualized as heatmaps using R scripts.

ANA ELISA

The nuclear antigen cocktail ELISA was performed according to the manufacturer's instructions using the ANA Screen ELISA Kit (Eagle Biosciences, catalog no. 4010), which included a cocktail of SLE antigens including Sm, ribonucleoprotein (RNP)/Sm, Scl-70, SS-A (Ro) (52 and 60 kDa), SS-B (La), Jo1, U1-SmRNP, centromere protein B (CENP-B), dsDNA, and histones. Individual mAbs were added at a concentration of 10 μg/ml for 1 hour at room temperature, washed with PBST three times, and incubated with HRP-conjugated anti-human IgG secondary antibody (Invitrogen, catalog no. 31410; 1:5000 dilution) for 30 min at room temperature. Plates were washed three times with PBST, and TMB substrate was added in the dark for 15 min at room temperature. The enzyme reaction was stopped by adding Stop solution as described above, and OD_{450} values were read on a BioTek Synergy H1 Multiplate Reader. An ANA negative mAb was run on each ELISA plate as an internal negative control to account for plate-to-plate background variability. The final OD_{450} values were normalized by subtracting the negative control mAb OD_{450} values from each of the tested mAbs OD_{450} values. Background subtracted OD_{450} values were visualized as heatmaps using R scripts.

Biolayer interferometry

Association and dissociation constants of mAbs to antigens were measured using biolayer interferometry on an Octet QK system (Fortebio/Sartorius) using the manufacturer's protocols. mAbs were bound to anti-hIgG Fc capture (AHC) biosensors, and antigens were used as analytes. After an initial titration experiment, mAb concentrations of 5 and 2.5 nM were selected. Antigen analytes were used at concentrations ranging from 32 to 500 nM for kinetic experiments. Data were analyzed using BLI software (Fortebio/Sartorius, v7.1), and GraphPad Prism 8.0 was used to generate the figures. Buffer controls were subtracted, and curves were fitted using all concentrations of the same ligand. Association/dissociation curves were generated using GraphPad Prism 8.0.

EBNA2 ChIP-seq, ATAC-seq, and RNA polymerase II occupancy data analysis

We analyzed publicly available EBNA2 ChIP-seq datasets from the National Center for Biotechnology Information Sequence Read Archive with accession numbers PRJNA141377 (for IB4 LCL), PRJNA624139 (for GM12878 LCL), PRJNA206727 (for Mutu-III), and PRJNA1031208 (for coactivators ChIP-seq). RNA polymerase II ChIP-seq data for GM12878 LCL were obtained from the ENCODE project. To assess whether EBNA2 binding influences chromatin structure, we analyzed ATAC-seq data from EBNA2-expressing (B95.8) and EBNA2-deficient (P3HR1) Ramos cells (PRJNA624139) (*42*). Enriched peaks corresponding to EBNA2 ChIP-seq binding

sites were identified using MACS2 (*73*) with the following parameters: -g hs -q 0.01. Replicate datasets from each study were pooled prior to peak calling to enhance signal detection and minimize variability. The identified peaks were further filtered based on an FDR threshold of <0.01. We used the ChIPseeker R package (*74*) for annotation and to assign putative target genes to EBNA2 binding sites. The annotated peaks were mapped to the nearest TSS within a 3000-bp upstream or downstream window. To investigate the functional relevance of EBNA2 binding in activation program in EBV^+ SLE B cells, we intersected the DEGs from EBV^+ versus EBV^- SLE B cells with the annotated EBNA2 ChIP-seq peaks.

Generation of EBV^+ LCLs

EBV^+ LCLs were generated using standard protocols (*75*). Magnetically isolated B cells from SLE and HC PBMCs were infected with EBV strain B95-8 (VR-1492, American Type Culture Collection) and cultured in RPMI 1640 medium supplemented with 10% FBS and 1% penicillin-streptomycin. After 2 weeks of culture, clusters of EBV-infected cells were harvested and expanded for 2 to 4 weeks to generate sufficient numbers of LCLs for cryopreservation and use in the described experiments. The SLE LCL lines used in the experiments presented were composed of mixed IgM and IgG LCLs that did not encode anti-DNA antibodies.

Loading LCL with chromatin antigen

LCLs from patients with SLE (derived from patients with SLE who had serum anti-DNA antinuclear autoantibodies; the LCL lines themselves did not encode anti-DNA autoantibodies) or LCLs from HCs were loaded with chromatin using an adapted version of previously described methods (*46*). Briefly, frozen LCLs (derived from individual patients with SLE or HCs, with each patient LCL line containing a mix of IgM^+ and IgG^+ LCLs) were thawed and cultured for 3 days in RPMI 1640 culture medium. An anti-dsDNA mAb was expressed in house and conjugated with avidin using the Streptavidin Conjugation Kit–Lightning-Link (Abcam) following the manufacturer's instructions. One million LCLs were chromatin loaded using biotin-labeled anti-IgM/IgG antisera (1 μg/ml; Jackson ImmunoResearch) preconjugated with the avidin-labeled anti-dsDNA mAb (expressed and conjugated in-house) and CpG ODN 2006 (3 μg/ml; Invivogen). Thereafter, the loaded LCLs were washed three times with PBS prior to coculture with B and T cells. For control groups, LCLs were incubated with CpG without anti-IgM/IgG dsDNA antibodies.

EBV^+ LCL cocultures with autologous and allogeneic T and B cells

The loaded LCLs were cocultured with isolated B and T cells from the same patient with SLE who had anti-DNA autoantibodies (MHC-matched), T and B cells from a different patient with SLE who had anti-DNA autoantibodies (MHC-mismatched), or T and B cells from a healthy individual (MHC-mismatched). Briefly, frozen PBMCs were thawed at room temperature, and dead cells were removed using the EasySep Dead Cell Removal (Annexin V) Kit (STEMCELL Technologies) according to the manufacturer's protocol. B and T cells were then isolated from the PBMCs using magnetic negative selection. B cells were isolated using the EasySep Human B Cell Isolation Kit (STEMCELL Technologies), and T cells were isolated using the EasySep Human T Cell Isolation Kit (STEMCELL Technologies), based on the manufacturer's instructions.

Isolated B and T cells were cocultured with LCL in 96-well plates (1×10^5 cells per well) at a ratio of 10 LCLs:40 B cells:50 T cells. All cocultured cells were maintained in RPMI 1640 medium supplemented with 10% FBS, 1% penicillin-streptomycin, interleukin-2 (IL-2) (1000 IU/ml; PeproTech), IL-21 (100 ng/ml; PeproTech), B cell activating factor (BAFF) (1 μg/ml; Miltenyi Biotec), and purified mouse anti-human CD28 (5 μg/ml; BD Biosciences). The cells were cultured in a humidified incubator at 37°C with 5% CO_2 for 10 days. The culture medium was refreshed every 2 to 3 days. At day 10, cells were collected for scRNA-seq, and supernatants were collected for HEp-2 staining to detect ANA. Data presented are representative of two independent experiments.

scRNA-seq analysis of EBV^+ LCL cocultures

Collected cells at the indicated time points and treatment conditions were processed for scRNA-seq, EBV-seq, CITE-seq, and BCR and TCR VDJ-seq as described above. Cells from each sample and experimental time point were labeled using oligo-conjugated hashtag antibodies (HTOs) prior to pooling. Each pool contains a loading control without anti-IgM/IgG dsDNA (HTO 1), a loading with anti-IgM/IgG dsDNA (HTO 4 and 6), and a loading and coculture with unmatched MHC B and T cells derived from a different patient (HTO 7). Hashtag-labeled cells were pooled and processed together for CITE-seq. Demultiplexing of the pooled samples was performed using the HTODemux function in Seurat. Unsupervised clustering identified distinct clusters of LCLs based on increased EBV UMI counts, and B cells and T cells were based on B and T cell marker gene expression (fig. S14). For downstream analysis, non-LCL B cell subsets were reclustered based on newly identified variable genes and PCA to achieve high-resolution subclustering, distinguishing memory B cells, DN2 B cells, and plasmablasts (fig. S15). A similar approach was applied to $CD4^+$ T cells for reclustering into subsets of $CD4^+$ T cells, including T_{PH}, central memory (CM), and effector memory (EM) $CD4^+$ T cells.

Statistical analysis

We used the chi-square test to assess the distribution of categorical variables such as frequencies of EBV^+ cells across groups. Pearson's correlation coefficient analysis was used to assess the strength and direction of linear relationships between continuous variables. For comparisons involving more than two groups, the Kruskal-Wallis test was used as a nonparametric alternative to a one-way analysis of variance (ANOVA). For comparisons between two independent groups, we used the Mann-Whitney *U* test as a nonparametric test and the Student's *t* test when normality assumptions were met, as measured by the Shapiro-Wilk test. Differential gene expression analysis between groups was performed using the Wilcoxon rank sum test. All statistical tests were conducted using R software with a significance threshold set at $P < 0.05$. Multiple testing corrections were applied using the Benjamini-Hochberg method to control the FDR and determine the significance threshold.

Supplementary Materials

The PDF file includes:
Figs. S1 to S16

Other Supplementary Material for this manuscript includes the following:
Tables S1 to S4
Data file S1
MDAR Reproducibility Checklist

REFERENCES AND NOTES

1. *Epstein Barr Virus Volume 2*, vol. 391, *Current Topics in Microbiology and Immunology*, C. Münz, Ed. (Springer Cham, 2015).
2. Z. X. Li, S. Zeng, H. X. Wu, Y. Zhou, The risk of systemic lupus erythematosus associated with Epstein-Barr virus infection: A systematic review and meta-analysis. *Clin. Exp. Med.* **19**, 23–36 (2019).
3. N. R. Jog, J. A. James, Epstein Barr virus and autoimmune responses in systemic lupus erythematosus. *Front. Immunol.* **11**, 623944 (2021).
4. J. A. James, K. M. Kaufman, A. D. Farris, E. Taylor-Albert, T. J. Lehman, J. B. Harley, An increased prevalence of Epstein-Barr virus infection in young patients suggests a possible etiology for systemic lupus erythematosus. *J. Clin. Invest.* **100**, 3019–3026 (1997).
5. J. A. James, B. R. Neas, K. L. Moser, T. Hall, G. R. Bruner, A. L. Sestak, J. B. Harley, Systemic lupus erythematosus in adults is associated with previous Epstein-Barr virus exposure. *Arthritis Rheum.* **44**, 1122–1126 (2001).
6. N. R. Jog, K. A. Young, M. E. Munroe, M. T. Harmon, J. M. Guthridge, J. A. Kelly, D. L. Kamen, G. S. Gilkeson, M. H. Weisman, D. R. Karp, P. M. Gaffney, J. B. Harley, D. J. Wallace, J. M. Norris, J. A. James, Association of Epstein-Barr virus serological reactivation with transitioning to systemic lupus erythematosus in at-risk individuals. *Ann. Rheum. Dis.* **78**, 1235–1241 (2019).
7. R. A. Wood, L. Guthridge, E. Thurmond, C. J. Guthridge, J. M. Kheir, R. L. Bourn, C. A. Wagner, H. Chen, W. DeJager, S. R. Macwana, S. Kamp, R. Lu, C. Arriens, E. F. Chakravarty, A. Thanou, J. T. Merrill, J. M. Guthridge, J. A. James, Serologic markers of Epstein-Barr virus reactivation are associated with increased disease activity, inflammation, and interferon pathway activation in patients with systemic lupus erythematosus. *J. Transl. Autoimmun.* **4**, 100117 (2021).
8. D. A. Thorley-Lawson, Epstein-Barr virus: Exploiting the immune system. *Nat. Rev. Immunol.* **1**, 75–82 (2001).
9. A. J. Gross, D. Hochberg, W. M. Rand, D. A. Thorley-Lawson, EBV and systemic lupus erythematosus: A new perspective. *J. Immunol.* **174**, 6599–6607 (2005).
10. E. M. Miyashita, B. Yang, K. M. Lam, D. H. Crawford, D. A. Thorley-Lawson, A novel form of Epstein-Barr virus latency in normal B cells in vivo. *Cell* **80**, 593–601 (1995).
11. D. Lau, L. Y. Lan, S. F. Andrews, C. Henry, K. T. Rojas, K. E. Neu, M. Huang, Y. Huang, B. DeKosky, A. E. Palm, G. C. Ippolito, G. Georgiou, P. C. Wilson, Low CD21 expression defines a population of recent germinal center graduates primed for plasma cell differentiation. *Sci. Immunol.* **2**, eaai8153 (2017).
12. A. V. Rubtsov, K. Rubtsova, A. Fischer, R. T. Meehan, J. Z. Gillis, J. W. Kappler, P. Marrack, Toll-like receptor 7 (TLR7)-driven accumulation of a novel CD11c^{+} B-cell population is important for the development of autoimmunity. *Blood* **118**, 1305–1315 (2011).
13. D. Dai, S. Gu, X. Han, H. Ding, Y. Jiang, X. Zhang, C. Yao, S. Hong, J. Zhang, Y. Shen, G. Hou, B. Qu, H. Zhou, Y. Qin, Y. He, J. Ma, Z. Yin, Z. Ye, J. Qian, Q. Jiang, L. Wu, Q. Guo, S. Chen, C. Huang, L. C. Kottyan, M. T. Weirauch, C. G. Vinuesa, N. Shen, The transcription factor ZEB2 drives the formation of age-associated B cells. *Science* **383**, 413–421 (2024).
14. X. Gao, Q. Shen, J. A. Roco, B. Dalton, K. Frith, C. M. L. Munier, F. D. Ballard, K. Wang, H. G. Kelly, M. Nekrasov, J. S. He, R. Jaeger, P. Carreira, J. I. Ellyard, L. Beattie, A. Enders, M. C. Cook, J. J. Zaunders, I. A. Cockburn, Zeb2 drives the formation of CD11c^{+} atypical B cells to sustain germinal centers that control persistent infection. *Sci. Immunol.* **9**, eadj4748 (2024).
15. K. Rubtsova, A. V. Rubtsov, M. P. Cancro, P. Marrack, Age-associated B cells: A T-bet-dependent effector with roles in protective and pathogenic immunity. *J. Immunol.* **195**, 1933–1937 (2015).
16. C. M. Tipton, C. F. Fucile, J. Darce, A. Chida, T. Ichikawa, I. Gregoretti, S. Schieferl, J. Hom, S. Jenks, R. J. Feldman, R. Mehr, C. Wei, F. E. Lee, W. C. Cheung, A. F. Rosenberg, I. Sanz, Diversity, cellular origin and autoreactivity of antibody-secreting cell population expansions in acute systemic lupus erythematosus. *Nat. Immunol.* **16**, 755–765 (2015).
17. S. A. Jenks, K. S. Cashman, E. Zumaquero, U. M. Marigorta, A. V. Patel, X. Wang, D. Tomar, M. C. Woodruff, Z. Simon, R. Bugrovsky, E. L. Blalock, C. D. Scharer, C. M. Tipton, C. Wei, S. S. Lim, M. Petri, T. B. Niewold, J. H. Anolik, G. Gibson, F. E. Lee, J. M. Boss, F. E. Lund, I. Sanz, Distinct effector B cells induced by unregulated Toll-like receptor 7 contribute to pathogenic responses in systemic lupus erythematosus. *Immunity* **49**, 725–739.e6 (2018).
18. M. T. McClain, L. D. Heinlen, G. J. Dennis, J. Roebuck, J. B. Harley, J. A. James, Early events in lupus humoral autoimmunity suggest initiation through molecular mimicry. *Nat. Med.* **11**, 85–89 (2005).
19. V. Laurynenka, L. Ding, K. M. Kaufman, J. A. James, J. B. Harley, A high prevalence of anti-EBNA1 heteroantibodies in systemic lupus erythematosus (SLE) supports anti-EBNA1 as an origin for SLE autoantibodies. *Front. Immunol.* **13**, 830993 (2022).
20. M. E. Munroe, J. R. Anderson, T. F. Gross, L. L. Stunz, G. A. Bishop, J. A. James, Epstein-Barr functional mimicry: Pathogenicity of oncogenic latent membrane protein-1 in systemic lupus erythematosus and autoimmunity. *Front. Immunol.* **11**, 606936 (2020).
21. W. H. Robinson, S. Younis, Z. Z. Love, L. Steinman, T. V. Lanz, Epstein-Barr virus as a potentiator of autoimmune diseases. *Nat. Rev. Rheumatol.* **20**, 729–740 (2024).
22. J. B. Harley, X. Chen, M. Pujato, D. Miller, A. Maddox, C. Forney, A. F. Magnusen, A. Lynch, K. Chetal, M. Yukawa, A. Barski, N. Salomonis, K. M. Kaufman, L. C. Kottyan, M. T. Weirauch, Transcription factors operate across disease loci, with EBNA2 implicated in autoimmunity. *Nat. Genet.* **50**, 699–707 (2018).
23. E. D. SoRelle, N. M. Reinoso-Vizcaino, G. Q. Horn, M. A. Luftig, Epstein-Barr virus perpetuates B cell germinal center dynamics and generation of autoimmune-associated phenotypes in vitro. *Front. Immunol.* **13**, 1001145 (2022).
24. J. Dai, E. D. SoRelle, E. Heckenberg, L. Song, J. M. Cable, G. E. Crawford, M. A. Luftig, Epstein-Barr virus induces germinal center light zone chromatin architecture and promotes survival through enhancer looping at the BCL2A1 locus. *MBio* **15**, e0244423 (2024).
25. D. Siemer, J. Kurth, S. Lang, G. Lehnerdt, J. Stanelle, R. Küppers, EBV transformation overrides gene expression patterns of B cell differentiation stages. *Mol. Immunol.* **45**, 3133–3141 (2008).
26. S. S. Soldan, C. Su, M. C. Monaco, L. Yoon, T. Kannan, U. Zankharia, R. J. Patel, J. Dheekollu, O. Vladimirova, J. W. Dowling, S. Thebault, N. Brown, A. Clauze, F. Andrada, A. Feder, P. J. Planet, A. Kossenkov, D. E. Schaffer, J. Ohayon, N. Auslander, S. Jacobson, P. M. Lieberman, Multiple sclerosis patient-derived spontaneous B cells have distinct EBV and host gene expression profiles in active disease. *Nat. Microbiol.* **9**, 1540–1554 (2024).
27. E. D. SoRelle, L. E. Haynes, K. A. Willard, B. Chang, J. Ch'ng, H. Christofk, M. A. Luftig, Epstein-Barr virus reactivation induces divergent abortive, reprogrammed, and host shutoff states by lytic progression. *PLoS Pathog.* **20**, e1012341 (2024).
28. H. Vietzen, S. M. Berger, L. M. Kuhner, P. L. Furlano, G. Bsteh, T. Berger, P. Rommer, E. Puchhammer-Stockl, Ineffective control of Epstein-Barr-virus-induced autoimmunity increases the risk for multiple sclerosis. *Cell* **186**, 5705–5718.e13 (2023).
29. F. Laderach, I. Piteros, E. Fennell, E. Bremer, M. Last, S. Schmid, L. Rieble, C. Campbell, I. Ludwig-Portugall, L. Bornemann, A. Gruhl, K. Eulitz, P. Gueguen, J. Mietz, A. Muller, G. Pezzino, J. Schmitz, G. Ferlazzo, J. Mautner, C. Munz, EBV induces CNS homing of B cells attracting inflammatory T cells. *Nature* **646**, 171–179 (2025).
30. K. Rubtsova, A. V. Rubtsov, L. F. van Dyk, J. W. Kappler, P. Marrack, T-box transcription factor T-bet, a key player in a unique type of B-cell activation essential for effective viral clearance. *Proc. Natl. Acad. Sci. U.S.A.* **110**, E3216–E3224 (2013).
31. S. M. Lens, R. de Jong, B. Hooibrink, G. Koopman, S. T. Pals, M. H. van Oers, R. A. van Lier, Phenotype and function of human B cells expressing CD70 (CD27 ligand). *Eur. J. Immunol.* **26**, 2964–2971 (1996).
32. M. Maric, B. Arunachalam, U. T. Phan, C. Dong, W. S. Garrett, K. S. Cannon, C. Alfonso, L. Karlsson, R. A. Flavell, P. Cresswell, Defective antigen processing in GILT-free mice. *Science* **294**, 1361–1365 (2001).
33. J. Neefjes, M. L. Jongsma, P. Paul, O. Bakke, Towards a systems understanding of MHC class I and MHC class II antigen presentation. *Nat. Rev. Immunol.* **11**, 823–836 (2011).
34. P. M. Kloetzel, Antigen processing by the proteasome. *Nat. Rev. Mol. Cell Biol.* **2**, 179–188 (2001).
35. P. T. Lange, B. Damania, Epstein-Barr virus-positive lymphomas exploit ectonucleotidase activity to limit immune responses and prevent cell death. *mBio* **14**, e0345922 (2023).
36. G. La Manno, R. Soldatov, A. Zeisel, E. Braun, H. Hochgerner, V. Petukhov, K. Lidschreiber, M. E. Kastriti, P. Lonnerberg, A. Furlan, J. Fan, L. E. Borm, Z. Liu, D. van Bruggen, J. Guo, X. He, R. Barker, E. Sundstrom, G. Castelo-Branco, P. Cramer, I. Adameyko, S. Linnarsson, P. V. Kharchenko, RNA velocity of single cells. *Nature* **560**, 494–498 (2018).
37. V. Bergen, M. Lange, S. Peidli, F. A. Wolf, F. J. Theis, Generalizing RNA velocity to transient cell states through dynamical modeling. *Nat. Biotechnol.* **38**, 1408–1414 (2020).
38. M. J. McClellan, C. D. Wood, O. Ojeniyi, T. J. Cooper, A. Kanhere, A. Arvey, H. M. Webb, R. D. Palermo, M. L. Harth-Hertle, B. Kempkes, R. G. Jenner, M. J. West, Modulation of enhancer looping and differential gene targeting by Epstein-Barr virus transcription factors directs cellular reprogramming. *PLOS Pathog.* **9**, e1003636 (2013).
39. B. Zhao, J. Zou, H. Wang, E. Johannsen, C. W. Peng, J. Quackenbush, J. C. Mar, C. C. Morton, M. L. Freedman, S. C. Blacklow, J. C. Aster, B. E. Bernstein, E. Kieff, Epstein-Barr virus exploits intrinsic B-lymphocyte transcription programs to achieve immortal cell growth. *Proc. Natl. Acad. Sci. U.S.A.* **108**, 14902–14907 (2011).
40. K. Viel, S. Parameswaran, O. A. Donmez, C. R. Forney, M. R. Hass, C. Yin, S. H. Jones, H. K. Prosser, A. A. Diouf, O. E. Gittens, L. E. Edsall, X. Chen, H. Rowden, K. A. Dunn, R. Guo, A. VonHandorf, M. M. L. Leong, K. Ernst, K. M. Kaufman, L. P. Lawson, B. Gewurz, B. Zhao, L. C. Kottyan, M. T. Weirauch, Shared and distinct interactions of type 1 and type 2 Epstein-Barr nuclear antigen 2 with the human genome. *BMC Genomics* **25**, 273 (2024).
41. E. D. SoRelle, N. M. Reinoso-Vizcaino, J. Dai, A. P. Barry, C. Chan, M. A. Luftig, Epstein-Barr virus evades restrictive host chromatin closure by subverting B cell activation and germinal center regulatory loci. *Cell Rep.* **42**, 112958 (2023).
42. T. Hong, S. Parameswaran, O. A. Donmez, D. Miller, C. Forney, M. Lape, M. S. J. Ribeiro, J. Liang, L. E. Edsall, A. F. Magnusen, W. Miller, I. Chepelev, J. B. Harley, B. Zhao, L. C. Kottyan, M. T. Weirauch, Epstein-Barr virus nuclear antigen 2 extensively rewires the human chromatin landscape at autoimmune risk loci. *Genome Res.* **31**, 2185–2198 (2021).
43. S. Jiang, H. Zhou, J. Liang, C. Gerdt, C. Wang, L. Ke, S. C. S. Schmidt, Y. Narita, Y. Ma, S. Wang, T. Colson, B. Gewurz, G. Li, E. Kieff, B. Zhao, The Epstein-Barr virus regulome in lymphoblastoid cells. *Cell Host Microbe* **22**, 561–573.e4 (2017).

44. S. Constant, N. Schweitzer, J. West, P. Ranney, K. Bottomly, B lymphocytes can be competent antigen-presenting cells for priming $CD4^+$ T cells to protein antigens in vivo. *J. Immunol.* **155**, 3734–3741 (1995).
45. S. P. Lee, L. E. Wallace, M. Mackett, J. R. Arrand, P. F. Searle, M. Rowe, A. B. Rickinson, MHC class II-restricted presentation of endogenously synthesized antigen: Epstein-Barr virus transformed B cell lines can present the viral glycoprotein gp340 by two distinct pathways. *Int. Immunol.* **5**, 451–460 (1993).
46. S. Pawaria, K. Moody, P. Busto, K. Nundel, C. H. Choi, T. Ghayur, A. Marshak-Rothstein, Cutting edge: DNase II deficiency prevents activation of autoreactive B cells by double-stranded DNA endogenous ligands. *J. Immunol.* **194**, 1403–1407 (2015).
47. D. A. Rao, M. F. Gurish, J. L. Marshall, K. Slowikowski, C. Y. Fonseka, Y. Liu, L. T. Donlin, L. A. Henderson, K. Wei, F. Mizoguchi, N. C. Teslovich, M. E. Weinblatt, E. M. Massarotti, J. S. Coblyn, S. M. Helfgott, Y. C. Lee, D. J. Todd, V. P. Bykerk, S. M. Goodman, A. B. Pernis, L. B. Ivashkiv, E. W. Karlson, P. A. Nigrovic, A. Filer, C. D. Buckley, J. A. Lederer, S. Raychaudhuri, M. B. Brenner, Pathologically expanded peripheral T helper cell subset drives B cells in rheumatoid arthritis. *Nature* **542**, 110–114 (2017).
48. E. Meffre, K. C. O'Connor, Impaired B-cell tolerance checkpoints promote the development of autoimmune diseases and pathogenic autoantibodies. *Immunol. Rev.* **292**, 90–101 (2019).
49. M. Larsen, D. Sauce, C. Deback, L. Arnaud, A. Mathian, M. Miyara, D. Boutolleau, C. Parizot, K. Dorgham, L. Papagno, V. Appay, Z. Amoura, G. Gorochov, Exhausted cytotoxic control of Epstein–Barr virus in human lupus. *PLOS Pathog.* **7**, e1002328 (2011).
50. I. Kang, T. Quan, H. Nolasco, S. H. Park, M. S. Hong, J. Crouch, E. G. Pamer, J. G. Howe, J. Craft, Defective control of latent Epstein-Barr virus infection in systemic lupus erythematosus. *J. Immunol.* **172**, 1287–1294 (2004).
51. E. Heath, N. Begue-Pastor, S. Chaganti, D. Croom-Carter, C. Shannon-Lowe, D. Kube, R. Feederle, H. J. Delecluse, A. B. Rickinson, A. I. Bell, Epstein-Barr virus infection of naive B cells in vitro frequently selects clones with mutated immunoglobulin genotypes: Implications for virus biology. *PLOS Pathog.* **8**, e1002697 (2012).
52. J. D. Fingeroth, J. J. Weis, T. F. Tedder, J. L. Strominger, P. A. Biro, D. T. Fearon, Epstein-Barr virus receptor of human B lymphocytes is the C3d receptor CR2. *Proc. Natl. Acad. Sci. U.S.A.* **81**, 4510–4514 (1984).
53. A. V. Bocharnikov, J. Keegan, V. S. Wacleche, Y. Cao, C. Y. Fonseka, G. Wang, E. S. Muise, K. X. Zhang, A. Arazi, G. Keras, Z. J. Li, Y. Qu, M. F. Gurish, M. Petri, J. P. Buyon, C. Putterman, D. Wofsy, J. A. James, J. M. Guthridge, B. Diamond, J. H. Anolik, M. F. Mackey, S. E. Alves, P. A. Nigrovic, K. H. Costenbader, M. B. Brenner, J. A. Lederer, D. A. Rao, Accelerating Medicines Partnership (AMP) RA/SLE Network, PD-$1^{hi}$$CXCR5^-$ T peripheral helper cells promote B cell responses in lupus via MAF and IL-21. *JCI Insight* **4**, e130062 (2019).
54. S. A. Jenks, K. S. Cashman, M. C. Woodruff, F. E. Lee, I. Sanz, Extrafollicular responses in humans and SLE. *Immunol. Rev.* **288**, 136–148 (2019).
55. H. Wardemann, S. Yurasov, A. Schaefer, J. W. Young, E. Meffre, M. C. Nussenzweig, Predominant autoantibody production by early human B cell precursors. *Science* **301**, 1374–1377 (2003).
56. E. D. SoRelle, J. Dai, N. M. Reinoso-Vizcaino, A. P. Barry, C. Chan, M. A. Luftig, Time-resolved transcriptomes reveal diverse B cell fate trajectories in the early response to Epstein-Barr virus infection. *Cell Rep.* **40**, 111286 (2022).
57. P. M. Bhende, S. J. Dickerson, X. Sun, W. H. Feng, S. C. Kenney, X-box-binding protein 1 activates lytic Epstein-Barr virus gene expression in combination with protein kinase D. *J. Virol.* **81**, 7363–7370 (2007).
58. D. Iwakiri, K. Takada, Role of EBERs in the pathogenesis of EBV infection. *Adv. Cancer Res.* **107**, 119–136 (2010).
59. C. Lin, J. Zong, W. Lin, M. Wang, Y. Xu, R. Zhou, S. Lin, Q. Guo, H. Chen, Y. Ye, B. Zhang, J. Pan, EBV-miR-BART8-3p induces epithelial-mesenchymal transition and promotes metastasis of nasopharyngeal carcinoma cells through activating NF-kappaB and Erk1/2 pathways. *J. Exp. Clin. Cancer Res.* **37**, 283 (2018).
60. S. Humme, G. Reisbach, R. Feederle, H. J. Delecluse, K. Bousset, W. Hammerschmidt, A. Schepers, The EBV nuclear antigen 1 (EBNA1) enhances B cell immortalization several thousandfold. *Proc. Natl. Acad. Sci. U.S.A.* **100**, 10989–10994 (2003).
61. J. T. Merrill, C. M. Neuwelt, D. J. Wallace, J. C. Shanahan, K. M. Latinis, J. C. Oates, T. O. Utset, C. Gordon, D. A. Isenberg, H. J. Hsieh, D. Zhang, P. G. Brunetta, Efficacy and safety of rituximab in moderately-to-severely active systemic lupus erythematosus: The randomized, double-blind, phase II/III systemic lupus erythematosus evaluation of rituximab trial. *Arthritis Rheum.* **62**, 222–233 (2010).
62. A. Mackensen, F. Muller, D. Mougiakakos, S. Boltz, A. Wilhelm, M. Aigner, S. Volkl, D. Simon, A. Kleyer, L. Munoz, S. Kretschmann, S. Kharboutli, R. Gary, H. Reimann, W. Rosler, S. Uderhardt, H. Bang, M. Herrmann, A. B. Ekici, C. Buettner, K. M. Habenicht, T. H. Winkler, G. Kronke, G. Schett, Anti-CD19 CAR T cell therapy for refractory systemic lupus erythematosus. *Nat. Med.* **28**, 2124–2132 (2022).
63. L. Bucci, S. Böltz, M. Hagen, C. Tur, D. M. Nöthling, T. Rothe, A. Wirsching, J. Auth, J. Wacker, M. Eckstein, S. Alivernini, A. Bozec, C. Bergmann, M. A. D'Agostino, L. Munoz, J. Rech, L. Kihm, M. G. Raimondo, G. Schett, R. Grieshaber-Bouyer, BCMA T-cell engager therapy in patients with refractory autoimmune disease. *N. Engl. J. Med.* **393**, 1544–1547 (2025).
64. R. Miskovic, A. Cirkovic, D. Miljanovic, I. Jeremic, M. Grk, M. Basaric, I. Lazarevic, M. Stojanovic, A. Plavsic, S. Raskovic, A. Banko, Epstein-Barr virus reactivation as a new predictor of achieving remission or lupus low disease activity state in patients with systemic lupus erythematosus with cutaneous involvement. *Int. J. Mol. Sci.* **24**, 6156 (2023).
65. A. S. Bais, D. Kostka, scds: Computational annotation of doublets in single-cell RNA sequencing data. *Bioinformatics* **36**, 1150–1158 (2020).
66. I. Korsunsky, N. Millard, J. Fan, K. Slowikowski, F. Zhang, K. Wei, Y. Baglaenko, M. Brenner, P. R. Loh, S. Raychaudhuri, Fast, sensitive and accurate integration of single-cell data with Harmony. *Nat. Methods* **16**, 1289–1296 (2019).
67. Y. Pan, J. T. Landis, R. Moorad, D. Wu, J. S. Marron, D. P. Dittmer, The Poisson distribution model fits UMI-based single-cell RNA-sequencing data. *BMC Bioinformatics* **24**, 256 (2023).
68. G. Yu, L. G. Wang, Y. Han, Q. Y. He, clusterProfiler: An R package for comparing biological themes among gene clusters. *OMICS* **16**, 284–287 (2012).
69. N. T. Gupta, J. A. Vander Heiden, M. Uduman, D. Gadala-Maria, G. Yaari, S. H. Kleinstein, Change-O: A toolkit for analyzing large-scale B cell immunoglobulin repertoire sequencing data. *Bioinformatics* **31**, 3356–3358 (2015).
70. N. T. Gupta, K. D. Adams, A. W. Briggs, S. C. Timberlake, F. Vigneault, S. H. Kleinstein, Hierarchical clustering can identify B cell clones with high confidence in Ig repertoire sequencing data. *J. Immunol.* **198**, 2489–2499 (2017).
71. K. P. Schliep, phangorn: Phylogenetic analysis in R. *Bioinformatics* **27**, 592–593 (2011).
72. S. Xu, L. Li, X. Luo, M. Chen, W. Tang, L. Zhan, Z. Dai, T. T. Lam, Y. Guan, G. Yu, *Ggtree*: A serialized data object for visualization of a phylogenetic tree and annotation data. *Imeta* **1**, e56 (2022).
73. Y. Zhang, T. Liu, C. A. Meyer, J. Eeckhoute, D. S. Johnson, B. E. Bernstein, C. Nusbaum, R. M. Myers, M. Brown, W. Li, X. S. Liu, Model-based analysis of ChIP-Seq (MACS). *Genome Biol.* **9**, R137 (2008).
74. G. Yu, L. G. Wang, Q. Y. He, ChIPseeker: An R/Bioconductor package for ChIP peak annotation, comparison and visualization. *Bioinformatics* **31**, 2382–2383 (2015).
75. Q. Y. Yao, H. Czarnecka, A. B. Rickinson, Spontaneous outgrowth of Epstein-Barr virus-positive B-cell lines from circulating human B cells of different buoyant densities. *Int. J. Cancer* **48**, 253–257 (1991).

Acknowledgments: We thank members of the Robinson laboratory for advice and discussions. We thank I. Sanz (Emory University) for guidance on classification of EBV^+ B cells. We thank the Stanford Rheumatic Diseases Biorepository for collection and provision of samples from patients with SLE and healthy comparators. Clinical and sample data were collected and managed using REDCap electronic data capture tools hosted at Stanford University. **Funding:** This work was supported by National Institutes of Health (NIH) grant R01 R01AR078268 (to W.H.R. and D.E.O.), NIH grant R01 AI173189-01 (to T.V.L. and W.H.R.), NIH grant PATHO-PH2-SUB_17_23 (to W.H.R. and P.J.U.), NIH sub from R01AI024717, US Department of Veterans Affairs Merit Award I01BX006254 and Congressionally Directed Medical Research grant 14290452 (log # AT240092) (to J.B.H.), the Henry Gustav Floren Trust, the Stanford Department of Medicine Team Science Program, the Stanford Medicine Office of the Dean, NIH grant R01 AI182319-01, and NIH grant R01 AI 175771-01 (to P.J.U.), a Lupus Research Alliance grant (to T.V.L. and W.H.R.), and a Wallenberg Foundation fellowship and a Lupus Research Alliance career development award (to S.Y.). Support was also provided from the Brennan family and the Arthritis Research Coalition (ARC) (to W.H.R.). **Author contributions:** S.Y. and W.H.R. conceptualized the study. S.Y., S.I.M., S.R., S.J., and W.H.R. developed the methodology. S.Y., S.I.M., S.R., S.J., M.P., X.W., S.A., O.S., T.U.W., M.L.H., E.Y.Y., Y.C., S.P., and M.C.B. performed experiments. S.Y. and W.H.R. visualized the data. S.Y., D.E.O., T.V.L., P.J.U, and W.H.R. acquired funding. S.Y. and W.H.R. performed project administration and supervised the project. S.Y. and W.H.R. wrote the original draft of the manuscript. S.Y., D.E.O., P.J.U., J.B.H., E.M., L.S., A.M.-R., J.A.J., O.M.M., T.V.L., and W.H.R. reviewed and edited the manuscript. **Competing interests:** S.Y., M.P., and W.H.R. are inventors on a patent application USPTO 63/814,223 entitled "Targeting EBV-infected B cells for the treatment of EBV-associated autoimmune diseases," and T.V.L. and W.H.R. are co-inventors on USPTO 63/709,335 entitled "Targeting Epstein-Barr virus (EBV) RNAs with an RNA sensor to deplete EBV-transformed cells and treat EBV-associated diseases". S.Y., T.V.L., M.P., and W.H.R. are cofounders and stockholders in Ebvio Inc. T.V.L. and W.H.R. are cofounders and stockholders in Flatiron Bio LLC. W.H.R. is a director of Ebvio Inc. and of Flatiron Bio LLC. **Data and materials availability:** All data associated with this study are present in the paper or the Supplementary Materials. Tabulated data underlying all figures where $n < 20$ are provided in data file S1. The scRNA-seq datasets generated and analyzed in this study have been uploaded to the SequenceRead Archive (www.ncbi.nlm.nih.gov/sra) with the accession number PRJNA1301449.

Submitted 11 April 2025
Accepted 6 October 2025
Published 12 November 2025
10.1126/scitranslmed.ady0210